ELSEVIER

Chemical Geology 237 (2007) 211–232

CHEMICAL GEOLOGY
INCLUDING
ISOTOPE GEOSCIENCE

www.elsevier.com/locate/chemgeo

Carbon isotope chemostratigraphy of the Middle Riphean type section (Avzyan Formation, Southern Urals, Russia): Signal recovery in a fold-and-thrust belt

Julie K. Bartley [a,*], Linda C. Kah [b], Julie L. McWilliams [a,1], Alice F. Stagner [a,2]

[a] *Department of Geosciences, University of West Georgia, Carrollton, GA 30118, United States*
[b] *Department of Earth and Planetary Sciences, University of Tennessee, Knoxville, TN 37996, United States*

Received 9 July 2004; accepted 8 June 2006

Editor: P. Deines

Abstract

The Avzyan Formation of the southern Ural Mountains, Russia, forms part of the Middle Riphean (~1300–1000 Ma) type section. Its age is constrained to be younger than 1348 Ma and older than 1080 Ma and thus may preserve all or part of the mid-Mesoproterozoic isotopic shift. This shift represents a significant reorganization of the carbon cycle and separates pre-1300 Ma carbonates with $\delta^{13}C$ near 0‰ from post-1200 Ma Mesoproterozoic successions having average $\delta^{13}C$ values greater than +3.5‰.

Because the Avzyan Formation is a significant reference section for the Mesoproterozoic and because it has the potential to record this mid-Mesoproterozoic shift, a chemostratigraphic profile was constructed for this strongly folded and thrust-faulted succession. Best-preserved $\delta^{13}C$ values from carbonates of the Avzyan Formation lie mainly between 0‰ and +2‰, but the unit contains a single excursion, represented by several data points, to values greater than +4‰. The chemostratigraphy of the Avzyan Formation does not provide a definitive match to a better-dated succession; however, the character of the carbon isotopic curve is most similar to that of the Dismal Lakes Group, arctic Canada, suggesting that the Avzyan Formation was deposited during the mid-Mesoproterozoic isotopic shift and may have an age near 1270 Ma. Best-preserved Sr isotopic values of 0.70587 are also consistent with a later Mesoproterozoic age.

Keywords: Mesoproterozoic; Russia; Urals; Carbonate; Middle Riphean; Chemostratigraphy

1. Introduction

Carbon isotope chemostratigraphy has become an invaluable tool for evaluating ancient sedimentary successions. The utility of chemostratigraphy, however, depends strongly upon the robustness of the global chemostratigraphic reference curve. For the Neoproterozoic and Phanerozoic, this curve is reasonably well constrained and has been successfully used for time-correlation of sedimentary sequences (Kaufman and Knoll, 1995; Brasier et al., 1996; Kaufman et al., 1997; Halverson 2006; Maloof 2005–6), for placing temporal constraints on paleotectonic/paleoceanographic/paleoclimatic events (Derry et al., 1992; Kaufman et al., 1993, 1997; Saltzman, 2003), and for evaluating the mechanisms

* Corresponding author. Tel.: +1 678 839 4054; fax: +1 678 839 4071.
E-mail address: jbartley@westga.edu (J.K. Bartley).
[1] Presently at: School of Geology and Geophysics, University of Oklahoma, Norman, OK 73019, Japan.
[2] Presently at: S&ME, Inc., 3380 Town Point Drive, Ste. 140, Kennesaw, GA 30144, USA.

0009-2541/$ - see front matter © 2006 Elsevier B.V. All rights reserved.
doi:10.1016/j.chemgeo.2006.06.018

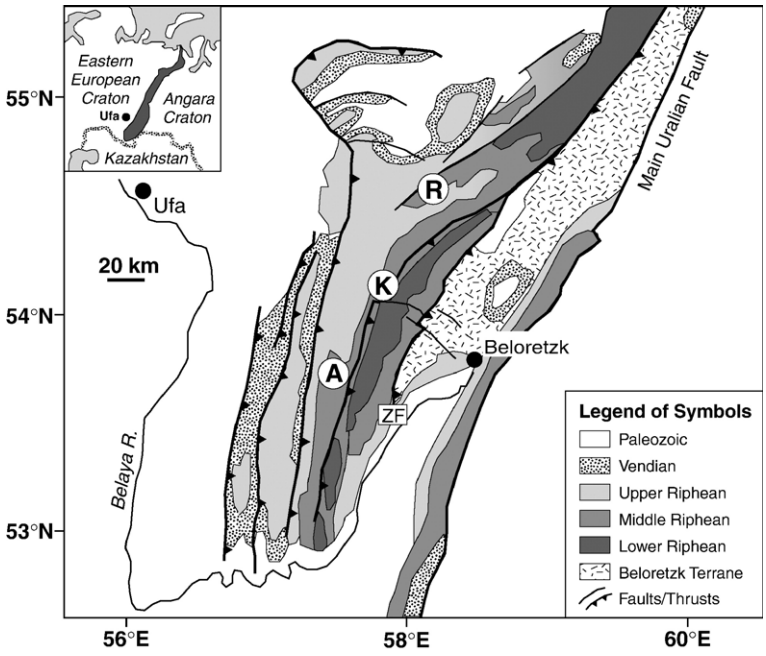

Fig. 1. Regional geologic map of the Bashkirian uplift, Southern Urals, Russia, modified from Giese et al. (1999) and Glasmacher et al. (2001). Riphean and Vendian strata occur as broadly developed open folds in a series of thrust sheets west of the Main Uralian Fault. East of the Zuratkul Fault (ZF), the Beloretzk Terrane represents overthrusting of moderate-to-high grade metamorphic rocks atop equivalent aged, low-grade strata to the west. Carbonate rocks for isotopic and elemental analysis were collected from measured sections of the Avzyan Formation at the Avzyan (A), Kataskin (K), and Katav River (R) sections, located near the towns of Verchney–Avzyan, Inzer, and Katav–Ivanovsk, respectively.

of biological and geochemical change in the geologic record (Derry et al., 1994; Saltzman et al., 1995; Montañez et al., 1996; Bartley et al., 1998). For older intervals, global reference curves are still evolving.

The Mesoproterozoic Era (1600 to 1000 Ma) represents a critical period in Earth history from the standpoint of global tectonic reorganisation (Hoffman, 1989, 1991; Dalziel, 1991; Karlstrom et al., 2001), the redox state of the oceans (Des Marais et al., 1992; Canfield and Teske, 1996; Canfield, 1998; Kah et al., 2004), the carbonate saturation state of the ocean (Grotzinger, 1989; Kah and Knoll, 1996; Bartley et al., 2000; Kah et al., 2001; Bartley and Kah, 2004), eukaryotic diversification (Knoll, 1992; Anbar and Knoll, 2002), and the advent of multicellularity (Butterfield et al., 1990; Woods et al., 1998; Butterfield, 2000). Recent work in these successions has improved constraints of age, depositional environment and post-depositional history, resulting in the first evaluations of broad-scale secular variation in the Mesoproterozoic marine carbon isotope system (Buick et al., 1995; Knoll et al., 1995; Xiao et al., 1997; Frank et al., 1997; Kah et al., 1999b; Lindsay and Brasier, 2000; Bartley et al., 2001; Frank et al., 2003). Whereas previous workers have described the Mesoproterozoic $\delta^{13}C$ record as uneventful (Buick et al., 1995; Brasier and Lindsay, 1998), a more recent and extensive compilation of data (Kah et al., 1999b) indicates that the Mesoproterozoic can be divided into two distinct intervals based on the variation and magnitude of $\delta^{13}C$ values in the marine carbonate record. Early Mesoproterozoic marine carbonates exhibit uniform carbon isotope compositions ($\delta^{13}C = 0.0 \pm 1.0‰$), consistent with prolonged stability of the marine carbon cycle between 1600 and ~1300 Ma. Carbonate strata younger than ~1200 Ma are characterized by higher $\delta^{13}C$ values ($\delta^{13}C = +3.5 \pm 1.0‰$). The mid-Mesoproterozoic shift to higher $\delta^{13}C$ values occurred between 1300 Ma and 1250 Ma (Frank et al., 2003) and suggests a fundamental change in ocean chemistry that persisted throughout the latter half of the Mesoproterozoic. Although it is clear that these first-order variations are of broad chronostratigraphic utility (Kah et al., 1999b; Bartley et al., 2001), additional data are needed to more precisely constrain the timing and nature of the mid-Mesoproterozoic carbon isotope shift and to interpret its significance with regard to global-scale processes.

Previous chemostratigraphic studies of Mesoproterozoic carbonates have focused on well-exposed, well-preserved epicratonal platform successions (e.g., Fairchild et al., 1990; Xiao et al., 1997; Bartley et al., 2000; Kah, 2000). Although these platform successions

commonly preserve highly reliable geochemical proxies for seawater, they commonly lack features (ash beds, igneous intrusions) useful in constraining geochronology. The type Riphean succession in the Southern Urals has been well studied geochronometrically, but as part of a craton margin sequence, these rocks have experienced a complex post-depositional history (Maslov et al., 1997). The aim of the present study is to reconstruct carbon isotopic change through the Avzyan Formation and to compare it to successions of broadly similar age, with the goal of better constraining a Mesoproterozoic carbon isotopic reference curve.

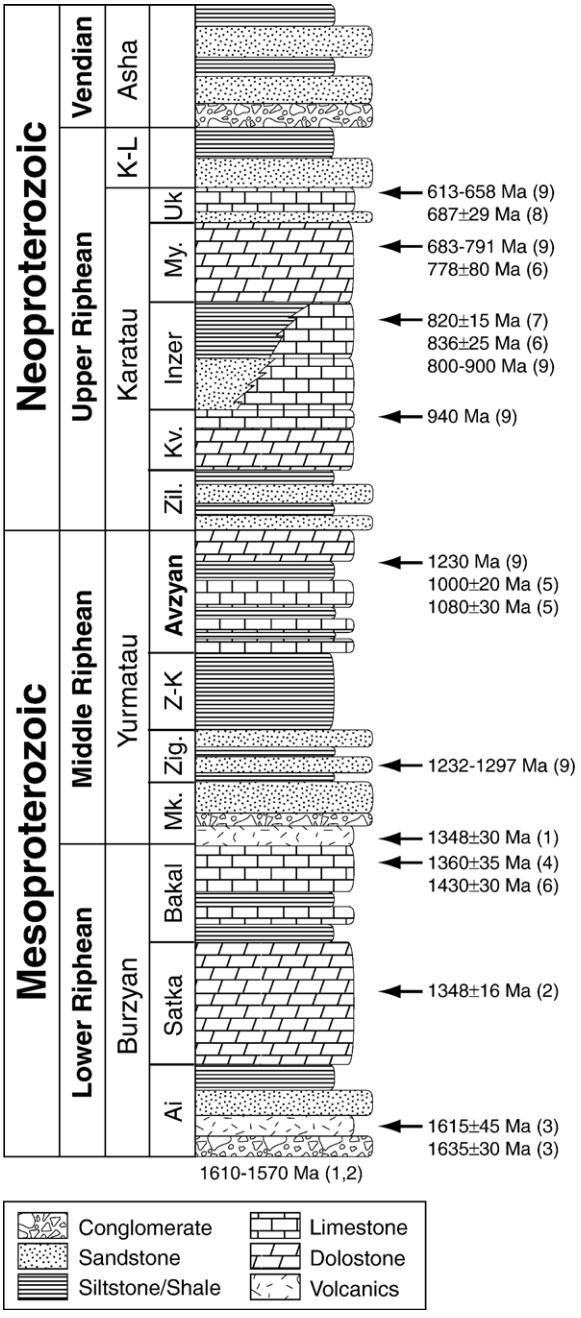

2. Riphean of the Southern Urals

2.1. Proterozoic strata of the Bashkirian uplift

The Bashkirian uplift, located between the town of Ufa, Russia and the Main Uralian Fault, is a complex structural terrane that comprises the western fold and thrust belt of the Southern Urals (Brown et al., 1997; Giese et al., 1999; Fig. 1). In the western Bashkirian uplift, greater than 15 km of Riphean and Vendian sedimentary and volcano-sedimentary strata are exposed in broad, open folds in a series of west-directed thrust sheets (Giese et al., 1999). Whereas Riphean and Vendian strata of the western uplift are typically unmetamorphosed to weakly metamorphosed (Matenaar et al., 1999), the Zuratkul Fault (Fig. 1) marks a major structural and metamorphic break wherein rocks of the eastern uplift (Beloretzk Terrane, Fig. 1) show polyphase deformation and an increase in metamorphic grade to greenschist- to eclogite-facies (Glasmacher et al., 2001).

Sedimentary strata of the western Bashkirian uplift include the Burzyan, Yurmatau, and Karatau groups, which represent the stratotype sections for the Lower, Middle, and Upper Riphean, respectively (Keller and Chumakov, 1983), and the Vendian Asha Group, which angularly overlies Riphean strata (Fig. 2). Each Riphean group is characterized by a basal unconformity overlain by coarse-grained, alluvial to marine siliciclastic sediments, frequently interrupted by volcanogenic deposits, that fine upward and are subsequently replaced by marine to evaporative marine limestones and dolostones (Keller and Chumakov, 1983; Kozlov et al., 1989; Maslov, 1994; Maslov et al., 1997; Maslov, 2002). The

Fig. 2. Generalized stratigraphic column of Riphean and Vendian (Meso- to Neoproterozoic) strata of the Southern Urals, Russia (modified from Keller and Chumakov, 1983), with current geochronological constraints. K–Ar analysis of diabase sills and early diagenetic glauconite suggest an age of ~1230–1000 Ma for the Avzyan Formation. Unit abbreviations: Krivaya Luka Group (K–L), Mashak Formation (Mk), Zigalga Formation (Zig), Zigazino–Komorovo Formation (Z–K), Zilmerdak Formation (Zil), Katav Formation (Kv), Minyar Formation (My). Geochronology abbreviations: U–$Pb_{diabase}$ (1), U–$Pb_{granite}$ (2), U–$Pb_{trachybasalt}$ (3), Rb–$Sr_{diabase}$ (4), K–$Ar_{diabase}$ (5), Pb–$Pb_{carbonate}$ (6), Rb–Sr_{illite} (7), Rb–$Sr_{glauconite}$ (8), K–$Ar_{glauconite}$ (9). Geochronologic data from: Keller and Chumakov (1983), Keller and Krasnobaev (1983), Ivanov et al. (1986), Kozlov et al. (1989), Gorokhov et al. (1995a,b), Gorozhanin (1995), Ovchinnikova et al. (1998), Ellmies et al. (2000), Kuznetsov et al. (2001).

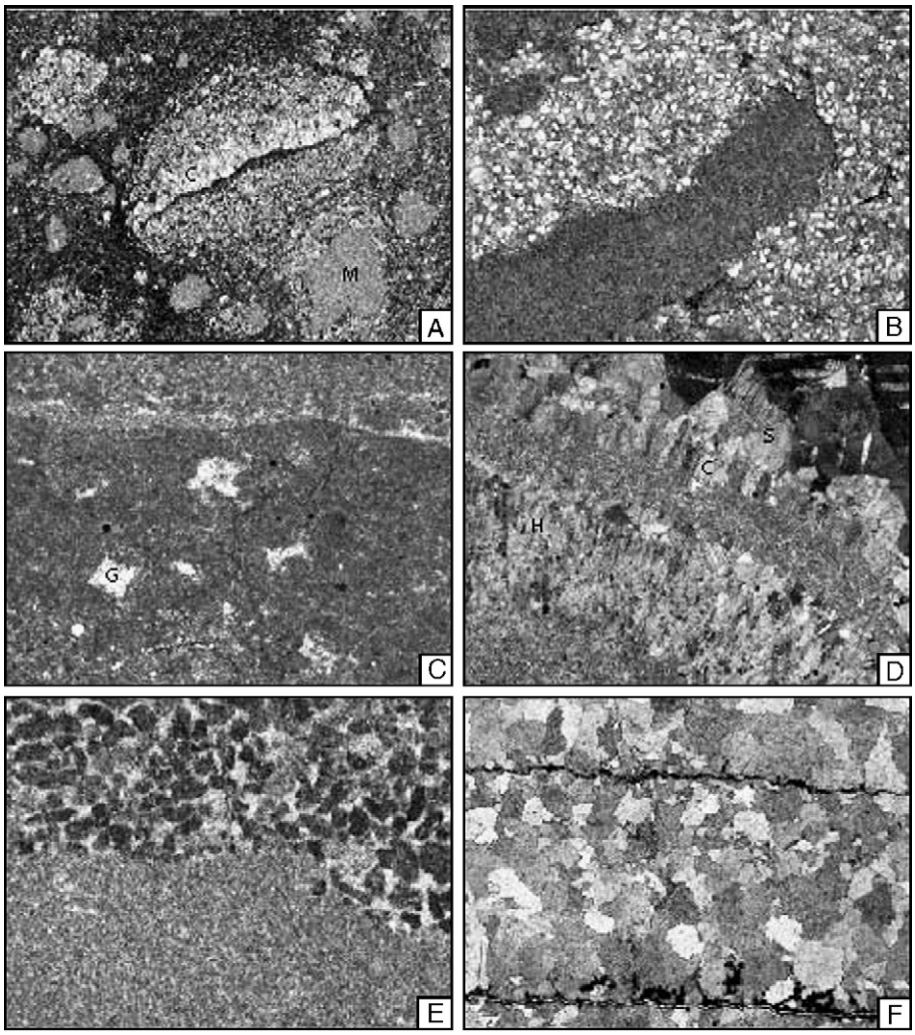

Fig. 3. Petrographic preservation of limestone, dolostone, and calcic dolostone lithologies of the Avzyan Formation. A. Limestone clasts in shaley matrix contain well-preserved micritic (m) and bladed, neomorphic cement (c) textures; B. Microsparitic limestone clast preserved in fine-grained quartz sandstone; C. Spar-filled gypsum molds in fine dolomite microspar; D. well-preserved herringbone (h), bladed (c), and sparry (s) cement textures in dolostone, observed in crossed-polarized light; E. detailed preservation in calcic dolostone of scour and fill with spar-cemented micritic intraclasts; F. fabric obliterative recrystallization of stromatolitic calcic dolostone, observed in crossed-polarized light. All photomicrographs are 2.58×3.45 mm. Well-preserved petrographic fabrics occur in both limestone and dolostone lithologies and, more rarely, in calcic dolostone lithologies. Poorly-preserved petrographic fabrics occur predominantly within calcic dolostones and correlate strongly with high degrees of geochemical overprinting.

Lower Riphean Burzyan Group consists, in stratigraphic order, of a variegated complex of oligomictic conglomerate, sandstone, silt, and trachybasalt of the Ai Formation; interbedded dolostone, black shale and silt of the Satka Formation; and variable interbedding of limestone, dolostone, and black shale of the Bakal Formation (Maslov, 1994). Similarly, Middle Riphean sedimentary strata of the Yurmatau Group consist of bimodal volcanics, conglomerate, and terrigenous sandstone of the Mashak Formation; shallow marine sandstone, silt and black shale of the Zigalga and Zigazino–Komorovo formations; and variable interbedding of limestone, dolostone, silt, and shale of the Avzyan Formation (Maslov, 2002). The Upper Riphean Karatau Group consists of basal arkosic sandstone and silt of the Zilmerdak Formation overlain by an assemblage of marine limestone, dolostone and minor terrigenous components of the Katav, Inzer, Minyar, and Uk formations (Maslov, 2002).

Riphean strata were deposited during successive episodes of extension and subsidence along the eastern margin of the East European Platform (EEP). Volcanic

rocks (trachybasalt, diabase, and bimodal basalt–rhyolite associations) suggest rifting in continental, transitional, to ocean settings (Maslov et al., 1997). Within the Bashkirian uplift, terrigenous facies typically thicken and coarsen westward and are characterized by continental platform provenance signatures, reflecting derivation primarily from the EEP (Willner et al., 2001). A regional angular unconformity at the base of the Vendian Asha Group and a change to easterly-derived terrigenous material marks the onset of convergence along the eastern margin of the EEP, broadly coeval with the exhumation and emplacement of the Beloretzk Terrane, and initiation of foreland basin deposition (Willner et al., 2003).

2.2. Geochronological constraints on Avzyan Formation deposition

In the Southern Urals, the age of the Middle Riphean Yurmatau Group is constrained by a variety of radiometric determinations (summarized in Fig. 2; Keller and Chumakov, 1983; Keller and Krasnobaev, 1983; Ivanov et al., 1986; Kozlov et al., 1989; Gorozhanin, 1995; Gorokhov et al., 1995a; Ovchinnikova et al., 1998; Ellmies et al., 2000; Kuznetsov et al., 2001) to have been deposited during the Late Mesoproterozoic, between approximately 1350 and 1000 Ma. Pb–Pb analyses of limestones in the underlying Bakal Formation (uppermost Burzyan Group) yield an age of 1430±30 Ma (Kuznetsov et al., 2001); diabase dikes that cut the Bakal Formation but do not intrude basal Yurmatau Group sediments give Rb–Sr ages of 1360±35 Ma (Ellmies et al., 2000). Geochronology of the Mashak volcanics (basal Yurmatau Group) yields a Rb–Sr age of 1341±41 Ma (Keller and Chumakov, 1983) and a U–Pb age of 1348±30 Ma (Kozlov et al., 1989). An upper age for Yurmatau Group strata is defined by K–Ar analysis on diabase dikes that intrude the Avzyan Formation (uppermost Yurmatau Group), which yield dates of 1000±20 Ma to 1080±30 Ma (Keller and Chumakov, 1983).

Although clearly older than 1000 Ma, the approximate age of cross-cutting diabase dikes (Keller and Chumakov, 1983), and younger than ~1350 Ma, the age of the Mashak Volcanics which lie >5 km beneath the Avzyan Formation at the base of the Yurmatau Group (Kozlov et al., 1989), the age of the Avzyan Formation itself remains poorly constrained. K–Ar analyses of early diagenetic glauconite in the upper Avzyan Formation yield an age of ~1230 Ma (Keller and Chumakov, 1983). However, no age constraints are available from the underlying Zigazino–Komorovo Formation and K–Ar ages of Avzyan glauconite are similar to the 1232–1297 Ma ages retrieved from glauconite in the Zigalga Formation, lower Yurmatau Group (Keller and Chumakov, 1983).

2.3. Stratigraphy and depositional setting of the Avzyan Formation

The present study examines the chemostratigraphy of the Avzyan Formation, and the following description derives from fieldwork conducted as part of this study (see Fig. 1 for localities visited). The Avzyan Formation conformably overlies organic-rich, shallow-marine shales and siltstones of the Zigazino–Komorovo Formation and marks the onset of marine carbonate deposition in the upper Yurmatau Group. The Avzyan Formation consists, in stratigraphic order, of the Kataskin, Malo Inzer, Ushakov, Kutkur, and Revet members, and is locally overlain by a sixth member, the Tyulmen Member, whose regional stratigraphic placement is uncertain (Kozlov et al., 1989). Although shallow marine throughout their extent (Maslov, 1989), stratigraphic thicknesses and lithologies of these members are variable (Keller and Chumakov, 1983), reflecting regional differences in subsidence, siliciclastic influx, and carbonate production.

The Kataskin Member (~450 m thick) consists of a series of grey- and orange-weathering limestone and dolostone intercalated with dark-coloured siltstone and shale. The basal 150 m are marked by a paucity of siliciclastic material and a greater proportion of dolostones. Carbonate sediments are typically fine-grained, finely laminated, and contain abundant molar-tooth structures, an enigmatic Precambrian carbonate fabric that consists of variously shaped voids and cracks filled with a uniform, equant microspar (O'Connor, 1972; Furniss et al., 1998; James et al., 1998; Pollock et al., 2006) and is generally restricted to shallow subtidal environments (James et al., 1998). Lower Kataskin strata are also marked by numerous beds and small bioherms of irregularly branching, columnar stromatolites. The upper 300 m of the Kataskin Member are characterized by 30–200 cm thick siliciclastic–carbonate cycles. In shale-rich intervals, limestones occur as discontinuous beds and nodules; in shale-poor intervals, limestones are present as amalgamated limestone beds with strongly scoured bases. A typical cycle consists of a lower horizon of black shale with abundant scours and an upper horizon of micritic limestone marked by development of mudcracks, microkarstic surfaces, flat-clast conglomerates and intraformational breccia, and occasionally oolitic and grainstone lithologies, indicating

deposition in regionally variable, shallow-marine, high-energy environments.

The Malo Inzer Member consists of ~175 m of intercalated micaceous siltstone, fine-grained sandstone, and black shale. Thin intervals of fine-grained, finely laminated dolostone occur near the base and rare, discontinuous stromatolitic bioherms occur higher in the section. Although minor scours and thin (2–7 cm thick) intervals of rippled and cross-bedded sandstone occur in the lower Malo Inzer, the predominance of flat-laminated facies, an upward increase in shaley lithologies, and moderate relief (20–60 cm) of stromatolitic bioherms suggests deposition in shallow subtidal conditions. The Malo Inzer is abruptly overlain by the ~150 m-thick Ushakov Member, dominated by tightly packed branching columnar, columnar, and conical stromatolite forms interbedded with dolomitic micrite and grainstone lithologies. The Ushakov is, in turn, overlain by the 60–150 m-thick Kutkur Member, which consists predominantly of grey–green micaceous siltstone.

The uppermost Avzyan Formation is represented by the Revet Member, which consists of massive to finely laminated, buff- to white-weathering dolostone with minor shale. The basal 50 m of the Revet Member at the Kataskin locality (cf. Fig. 1) consists of microbially laminated, fenestral dolostone containing abundant early diagenetic nodules of black chert. At the Avzyan locality, fenestral cherty facies are absent, and the base of the Revet consists predominantly of thinly bedded, shaley dolostone interbedded with 30–70 cm thick intervals of massively bedded, irregular, columnar stromatolites. Abruptly overlying basal biohermal facies, Revet facies shift to approximately 30 m of massively bedded, white-weathering carbonates that contain low-relief cuspate microbialites and intraformational breccia. Cuspate microbialites consist of an open network of draping lamina over thin, vertical supports and are similar to subtidal stromatolites reported from the Mesoproterozoic Dismal Lakes Group, arctic Canada (Kerans and Donaldson, 1989; Kah et al., 1999a). Like the Dismal Lakes cuspate microbialites, primary void space in Revet microbialites is filled with several cement generations, including herringbone carbonate (Sumner and Grotzinger, 1996a,b), bladed marine cement, and a late-stage dolomite spar (cf. Fig. 3D). Cuspate microbialites are overlain by approximately 50 m of non-cyclic, massively bedded dolomicrite capped by approximately 10 m of irregularly branching, columnar stromatolites. Strata of the uppermost Revet member consist predominantly of microbially laminated, fenestral dolostones that contain abundant intraformational breccias and early diagenetic chert, suggesting a return to peritidal deposition.

2.4. Lithologic descriptions

Samples for chemostratigraphic analysis were collected from measured stratigraphic sections of the uppermost Zigazino–Komorovo Formation and the carbonate-bearing Kataskin, Malo Inzer, and Revet members of the Avzyan Formation at the Avzyan and Kataskin localities (Fig. 1). Faulting has removed the Ushakov Member in the Avzyan locality and high water in the Inzer River precluded sampling of all but the uppermost Ushakov at the Kataskin locality. A second suite of Ushakov samples, collected from a measured stratigraphic section along the Katav River (Fig. 1), were provided by Dr. Vachyslav I. Kozlov of the Institute of Geology, Ufa, Russia.

Limestones of the Avzyan Formation typically reveal fine-scale preservation of depositional fabrics, including: 1) primary micritic and microsparitic lithologies, 2) grainstone lithologies, and 3) syndepositional marine cements (Fig. 3A, B). Where present, late-stage veins typically crosscut depositional facies with little or no visible effect on depositional fabrics. Most limestone facies are represented by homogeneous, unlaminated micrite and micrite containing discontinuous to continuous laminae of compacted organic material. In some cases, when organic material is abundant, originally micritic textures are interlaminated with elongate-to-bladed microspar crystals oriented perpendicular to organic-rich laminae. The distribution of bladed microspar textures, presence of organic inclusions within bladed microspar, and preservation of bladed microspar within sedimentary breccias (Fig. 3A) suggests an early diagenetic, neomorphic origin related to fluid flow along organic laminae. More frequently, however, primary micritic and fine microspar limestone textures are retained even in reworked grainstone lithologies (Fig. 3A, B).

Dolostones of the Avzyan Formation similarly show fine-scale preservation of depositional fabrics, suggesting early dolomitization in the presence of marine or modified-marine fluids (Montañez and Read, 1992; Kah, 2000). Dolostones are represented primarily by homogeneous unlaminated micrite, microbially laminated micritic and microspar, and grainstones composed of micritic intraclasts. However, several dolostone facies of the Revet Member preserve additional information about depositional environments. In the lowermost and uppermost Revet Member, peritidal dolostones frequently preserve spar-filled gypsum molds (Fig. 3C), indicating evaporitic depositional conditions. Similarly, replacive dolostones that comprise subtidal, cuspate microbialites of the middle Revet preserve at least three stages of isopachous cement growth prior to final occlusion of void

space by coarsely crystalline spar (Fig. 3D). The first cement stage is represented by herringbone carbonate, an unusual crystal morphology characterized by a c-axis that rotates during crystal growth (Sumner and Grotzinger, 1996a,b). In thin section, rotation of the c-axis is observed by a sweeping extinction along the long axis of the crystal. Although the origin of herringbone carbonate is uncertain, c-axis rotation may result from inhibition of crystal growth by Fe^{2+} in the precipitating fluid (Dromgoole and Walter, 1990), suggesting the presence of anoxic fluids. As in the Mesoproterozoic Dismal Lakes Group, arctic Canada (Kah et al., 1999a), and the Atar Group, Mauritania (Kah and Bartley, 2004), herringbone carbonate in the Revet Member occurs as a first-generation marine cement and is associated with a marine transgression that plausibly supplied suboxic to anoxic waters to the site of carbonate formation.

In contrast to stoichiometric dolostones, calcic dolostones in the Avzyan Formation show the most variable fabric preservation. Although fine-scale preservation of micritic and grainstone fabrics occurs (Fig. 3E), calcic dolostones more commonly are represented by coarse-grained, fabric-obliterative, neomorphic fabrics (Fig. 3F). Such fabric-obliterative textures are consistent with higher water–rock ratios and may also indicate prolonged isotopic exchange between rock and diagenetic fluids (Montañez and Read, 1992).

3. Methods

3.1. Geochemical Methods

Thin and polished thick sections of each carbonate hand sample were evaluated by optical and cathodoluminescence petrography to assess the range of carbonate fabrics for analysis. Where possible, multiple carbonate phases were sampled in order to provide a first-order assessment of depositional and/or diagenetic heterogeneity (cf. Kaufman et al., 1991; Kah et al., 1999b; Frank et al., 2003). Powdered samples (~2 mg) of individual carbonate phases were acquired from polished slabs using 0.3, 0.5, and 1.0 mm drill bits, in order to obtain subsamples that were petrographically homogeneous. Most samples were split for paired elemental and isotopic analysis; smaller samples were analyzed only for isotopic composition.

For carbon and oxygen isotopic analyses, drilled powders from the Revet Member at the Avzyan locality were reacted with >102% H_3PO_4 at 90 °C in evacuated, sealed tubes. Resultant carbon dioxide was distilled cryogenically into clean 6 mm Pyrex tubes and analyzed on a Finnigan MAT dual inlet gas source isotope ratio mass spectrometer at the University of Tennessee. All other samples were reacted on-line in individual reaction vessels with anhydrous phosphoric acid at 90 °C and analyzed using a Fisons Optima dual inlet gas source mass spectrometer at the University of California Davis or a VG Optima dual inlet gas source mass spectrometer housed at Mountain Mass Spectrometry, Inc. Oxygen isotope ratios were corrected for ^{17}O contribution (Craig, 1957). Fractionation factors used for calculation of ^{18}O abundances were 1.00798 for calcite and 1.00895 for dolomite, calculated by linear extrapolation of fractionation factors determined at 75 °C to the reaction temperature (90 °C) used in these analyses (Rosenbaum and Sheppard, 1986). On all instruments, precision is better than 0.1‰ for $\delta^{13}C$ and $\delta^{18}O$, based on multiple analyses of laboratory standards and isotopic composition is reported relative to the VPDB (Vienna Pee Dee Belemnite) standard.

In preparation for elemental analyses, aliquots of drilled powders were digested for 2 h in trace metal grade 2% HNO_3. Solutions were centrifuged and decanted to remove insoluble residue. Major (Ca, Mg) and trace (Mn, Sr, Fe) element analyses of carbonates were performed at the University of West Georgia using a Perkin-Elmer ICP-AES fitted with a Meinhardt concentric nebulizer. Precision and reproducibility for all elements analyzed are better than 10%, based on replicate measurements of laboratory calcite and dolomite standards.

For Sr isotopic analyses, <5 mg samples of powder were pretreated with ultrapure ammonium acetate to remove adsorbed and loosely bound Sr (Montañez et al., 1996). After removal of ammonium acetate, samples were dissolved in ultraclean 0.5 M acetic acid. Strontium was isolated from the resultant solution using Sr-Spec ion exchange resin. 500–1000 ng of purified Sr was then loaded onto a Ta filament with 1 μL TaO/H_2O slurry and dried to a small spot. Sr isotopic analysis was performed on the University of Maryland VG Sector 54 multicollector TIMS. Analyses were performed between 1450 and 1650 °C, typically using an ^{88}Sr signal of ~1V and >100 ratios. Multiple analyses of NBS-987 Sr standard run during the course of this investigation averaged 0.710242±0.000012 (uncertainty given as 2σ of the mean).

Shales collected from the Zigazino–Komarovo Formation and the Kataskin Member of the Avzyan Formation were processed for organic carbon isotopic analysis. Whole rock samples were crushed, and clean rock chips with no surface weathering were selected to be powdered using a Spex CertiPrep 8000 Mixer Mill equipped with an alumina ceramic vessel and milling balls. Powder (100–400 mg) was reacted with HCl in

Vycor tubing to remove carbonate. After rinsing, excess Cu/CuO was added to the sample. Tubes were sealed under vacuum and combusted at 850 °C to release CO_2, which was collected by cryogenic vacuum distillation. $\delta^{13}C$ values were determined on a Finnigan MAT dual inlet gas source isotope ratio mass spectrometer at the University of Tennessee. Analytical uncertainty is 0.2‰.

4. Results

4.1. Diagenesis

Because of the complex post depositional history of Avzyan carbonates, we expect that all samples will show geochemical evidence of alteration. However, numerous carbon isotopic studies of Paleozoic and Proterozoic carbonates have shown that carbon isotopic composition is less sensitive to diagenetic alteration than is $\delta^{18}O$ or trace element (Fe, Mn, Sr) composition as long as diagenetic fluids are relatively carbon-poor (Banner and Hanson, 1990; Kaufman et al., 1991; Banner and Kaufman, 1994). With this framework in mind, we expect tests of diagenesis in the Avzyan Formation to accomplish two goals: 1) to identify the *most* chemically altered samples — those that are least likely to preserve meaningful carbon isotopic signatures; and 2) to identify the *least* chemically altered samples — those that are most likely to preserve Sr isotopic composition.

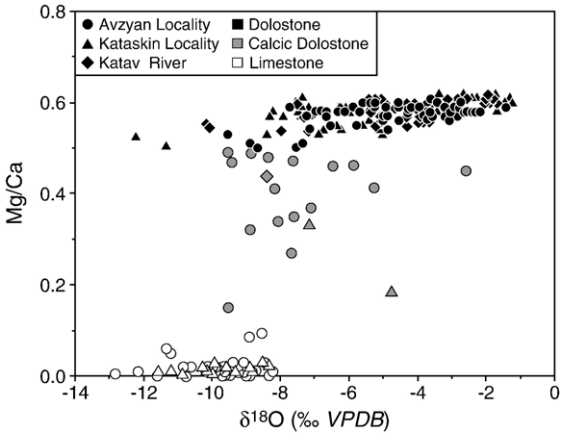

Fig. 4. Oxygen isotope compositions reveal strong partitioning with respect to mineralogy of sampled components. All samples show a range of oxygen isotopic composition, suggesting minor to moderate overprinting by diagenetic fluids. However, whereas intertidal to supratidal dolostones, which frequently show evidence of evaporitic deposition (cf. Fig. 3C), typically preserve the most positive isotopic compositions (near −2‰), shallow subtidal limestones and dolostones preserve more negative isotopic compositions (near −8‰), suggesting that primary depositional variation in marine isotopic composition also contributes to the observed spread of values. Well-preserved, non-evaporitic Precambrian carbonates frequently record oxygen isotope compositions between approximately −6‰ and −9‰ (Frank and Lyons, 2000; Kah, 2000).

Within the Avzyan Formation, we identify three classes of carbonate based on Mg/Ca ratio: limestone (Mg/Ca < 0.1), dolostone (Mg/Ca > 0.5; stoichiometric dolomite has Mg/Ca 0.6) and mixed (Mg/Ca 0.1 to 0.5). These three classes of carbonate in the Avzyan Formation also have distinct $\delta^{18}O$ characteristics (Fig. 4). $\delta^{18}O$ is a very sensitive indicator of diagenetic processes, even at low water:rock ratios (Banner and Hanson, 1990). Examination of $\delta^{18}O$ values by mineralogy reveals that dolostones are isotopically heavy, limestones have low $\delta^{18}O$ and carbonates with intermediate Mg/Ca ratios (0.1 to 0.5) have intermediate $\delta^{18}O$ values. These data permit two interpretations. If preserved $\delta^{18}O$ values are unaffected by diagenesis, it is possible that the observed isotopic difference is caused by equilibrium isotopic fractionation of oxygen between limestone and dolostone precipitating from a single fluid (Land, 1980). If the facies distribution of Avzyan carbonates is considered, however, a second alternative emerges. Whereas limestones of the Avzyan Formation represent shallow subtidal deposition, dolostones represent the shallowest carbonate facies, and preservation of gypsum molds and chert in Avzyan dolostones (Fig. 3C) further indicates the presence of episodically evaporitic marine environments. Because evaporitic seawater generally has higher $\delta^{18}O$ values than normal marine fluids (McKenzie et al., 1980), it is thus plausible that $\delta^{18}O$ values of Avzyan peritidal carbonates were originally higher than coeval subtidal carbonates and that early dolomitization of peritidal facies resulted in retention of isotopically heavier $\delta^{18}O$ values and fine-scale fabric retention. Subsequent diagenetic water–rock exchange is likely responsible for the observed scatter within $\delta^{18}O$ values for each rock type (Table 1), but the overall pattern may very well be a depositional one. Although evaporation sometimes (Stiller et al., 1985), but not always (Kah, 2000) produces ^{13}C enrichment, Avzyan dolomites are not systematically enriched in ^{13}C relative to limestones.

Poor preservation of $^{87}Sr/^{86}Sr$ values in both limestones and dolostones further indicates at least some exchange with diagenetic fluids. Sixteen samples were evaluated for $^{87}Sr/^{86}Sr$, and of these only a single point (KT(AZ)-63.8) had a strontium isotopic composition (0.705872) reminiscent of other measurements for Mesoproterozoic seawater (cf. Gorokhov et al., 1995b; Kah, 2000; Bartley et al., 2001). Overall, primary $^{87}Sr/^{86}Sr$ values are obliterated in the Avzyan Formation, and the lowest value of 0.705872 may be used only as an upper constraint on Mesoproterozoic seawater $^{87}Sr/^{86}Sr$ values, and not as a record of primary Sr isotopic composition.

Table 1
Isotopic and elemental compositions, Avzyan Formation carbonates (Avzyan Locality)

Sample‡	Member	Height‡‡ (m)	Mg/Ca (w/w)	$\delta^{13}C$ (‰ VPDB)	$\delta^{18}O$ (‰ VPDB)	Mn (ppm)	Fe (ppm)	Sr (ppm)	$^{87}Sr/^{86}Sr$
KT(AZ)-1	Kataskin	61.0	0.10	0.44	−8.55	2362	28,646	187	–
KT(AZ)-11.5	Kataskin	71.5	0.00	−0.19	−12.77	487	1541	331	–
KT(AZ)-15.3	Kataskin	75.3	0.05	−0.21	−11.21	944	6880	305	–
KT(AZ)-23	Kataskin	83.0	0.32	0.30	−8.89	7187	16,542	30	–
KT(AZ)-29.3*	Kataskin	89.3	0.44	−2.91	−8.46	5918	59,419	710	–
KT(AZ)-33.8	Kataskin	93.8	0.51	−0.21	−8.88	2810	61,466	932	0.71023
KT(AZ)-38.7	Kataskin	98.7	0.02	0.25	−9.23	413	3095	196	0.71472
KT(AZ)-43.4	Kataskin	103.4	0.47	0.36	−9.43	4168	63,299	98	–
KT(AZ)-49.5	Kataskin	109.5	0.50	−0.33	−8.67	3865	47,401	289	–
KT(AZ)-60.3	Kataskin	120.3	0.41	0.45	−8.17	2410	36,327	85	0.72678
KT(AZ)-63.8	Kataskin	123.8	0.01	0.49	−9.06	412	675	653	0.70587
KT(AZ)-82	Kataskin	142.0	0.06	−0.19	−11.34	780	9475	148	–
KT(AZ)-98-1*	Kataskin	158.0	0.46	−3.80	−10.80	4299	65,303	29	–
KT(AZ)-98-2*	Kataskin	158.0	0.16	0.84	−9.73	3398	23,130	75	–
KT(AZ)-131.6	Kataskin	191.6	0.53	0.19	−9.56	1624	31,796	54	–
KT(AZ)-141*	Kataskin	201.0	0.46	−1.79	−7.30	1218	36,439	85	–
KT(AZ)-201	Kataskin	304.0	0.35	0.41	−7.62	1184	29,602	145	–
KT(AZ)-212	Kataskin	315.0	0.01	0.24	−8.79	326	3407	171	–
KT(AZ)-219.1	Kataskin	322.1	0.01	−0.37	−8.22	332	3619	154	0.72843
KT(AZ)220-1	Kataskin	323.0	0.00	−0.53	−8.88	455	2349	119	–
KT(AZ)220-2*	Kataskin	323.0	0.00	−6.14	−8.77	536	4865	128	–
KT(AZ)-225.8	Kataskin	328.8	0.01	0.44	−8.70	709	6580	148	–
KT(AZ)-231-1	Kataskin	334.0	0.01	−0.21	−9.89	765	8961	128	–
KT(AZ)-231-2	Kataskin	334.0	0.01	−0.38	−9.61	1083	10,774	167	–
KT(AZ)-236-1	Kataskin	339.0	0.03	0.75	−9.40	684	10,876	163	–
KT(AZ)-236-2	Kataskin	339.0	0.02	0.69	−9.89	444	5933	248	0.72234
KT(AZ)-236-3	Kataskin	339.0	0.02	1.60	−10.11	699	10,829	168	–
KT(AZ)-244-1	Kataskin	347.0	0.02	0.36	−9.66	514	10,052	265	–
KT(AZ)-244-2	Kataskin	347.0	0.01	0.56	−9.71	538	7585	273	–
KT(AZ)-249	Kataskin	352.0	0.01	−0.49	−9.75	838	10,908	254	–
KT(AZ)-253-1	Kataskin	356.0	0.01	−0.49	−9.72	914	9387	217	–
KT(AZ)-253-2	Kataskin	356.0	–	−0.58	−10.22	–	–	–	–
KT(AZ)-264.8	kataskin	367.8	0.00	0.90	−9.69	1442	8323	166	–
KT(AZ)-273.3	Kataskin	376.3	0.02	1.06	−10.83	477	12,348	259	0.74182
KT(AZ)-281	Kataskin	384.0	0.34	1.98	−8.08	1148	52,430	156	–
KT(AZ)-285	Kataskin	388.0	0.09	2.11	−8.91	399	8304	296	–
KT(AZ)-290.3	Kataskin	393.3	0.01	0.91	−8.82	534	9256	254	–
KT(AZ)-296	Kataskin	399.0	0.01	−0.40	−12.16	287	4486	220	0.72564
KT(AZ)-307	Kataskin	410.0	0.41	1.75	−5.26	1446	64573	204	–
KT(AZ)-315.5	Kataskin	418.5	0.03	1.10	−8.47	408	10,844	265	0.73184
KT(AZ)-322	Kataskin	425.0	0.00	2.12	−8.35	156	715	416	–
KT(AZ)-328-1	Kataskin	431.0	0.03	1.90	−9.10	494	5759	249	–
KT(AZ)-328-2	Kataskin	431.0	0.01	2.58	−8.82	181	1829	401	–
KT(AZ)-328-3	Kataskin	431.0	0.27	2.63	−7.70	1395	35,812	161	–
KT(AZ)-328-4	Kataskin	431.0	–	1.55	−8.47	–	–	–	–
KT(AZ)-334	Kataskin	437.0	0.00	1.42	−9.00	590	4668	289	–
KT(AZ)-340	Kataskin	443.0	0.02	1.21	−9.35	298	4407	208	0.72158
KT(AZ)-346-1	Kataskin	449.0	0.01	3.65	−9.21	347	4362	295	–
KT(AZ)-346-2	Kataskin	449.0	0.01	4.49	−9.07	298	3780	285	0.71150
KT(AZ)-346-3	Kataskin	449.0	–	4.41	−9.88	–	–	–	–
KT(AZ)-352	Kataskin	455.0	0.01	1.48	−9.96	310	4073	268	0.72650
KT(AZ)-358-1	Kataskin	461.0	0.02	1.24	−9.96	609	4286	300	–
KT(AZ)-358-3	Kataskin	461.0	–	0.45	−10.23	–	–	–	–
KT(AZ)-358-4	Kataskin	461.0	–	0.55	−10.33	–	–	–	–
KT(AZ)-373.5	Kataskin	476.5	0.01	1.02	−9.87	1184	13,780	594	–
KT(AZ)-379-1	Kataskin	482.0	0.01	1.00	−10.02	531	5920	569	0.72139
KT(AZ)-379-2	Kataskin	482.0	0.01	1.33	−10.18	670	8388	520	–

(continued on next page)

Table 1 (*continued*)

Sample‡	Member	Height‡‡ (m)	Mg/Ca (w/w)	$\delta^{13}C$ (‰ VPDB)	$\delta^{18}O$ (‰ VPDB)	Mn (ppm)	Fe (ppm)	Sr (ppm)	$^{87}Sr/^{86}Sr$
KT(AZ)-379-3*	Kataskin	482.0	0.02	1.14	−10.61	1323	17,162	442	–
KT(AZ)-383-1	Kataskin	486.0	0.01	2.79	−9.69	622	4182	282	–
KT(AZ)-383-2	Kataskin	486.0	0.15	2.90	−9.49	1521	24,097	181	–
KT(AZ)-383-3	Kataskin	486.0	–	2.69	−12.35	–	–	–	–
KT(AZ)-392-1	Kataskin	495.0	0.00	2.62	−9.48	307	3097	811	–
KT(AZ)-392-2	Kataskin	495.0	0.00	3.36	−9.57	474	1607	450	–
MI(AZ)-413	MaloInzer	527.5	0.00	1.58	−11.58	1047	3956	269	–
MI(AZ)-416-1	MaloInzer	530.5	0.00	1.79	−10.76	1175	2899	413	–
MI(AZ)-416-3	MaloInzer	530.5	0.01	1.67	−10.93	1808	3585	238	–
MI(AZ)-37	MaloInzer	605.5	0.51	0.81	−7.33	8981	31,542	91	–
MI(AZ)-39	MaloInzer	607.5	0.50	0.73	−7.56	8659	34,362	59	–
MI(AZ)-47	MaloInzer	615.5	0.47	0.50	−7.63	13033	49,535	70	–
MI(AZ)-49-1	MaloInzer	617.5	0.46	0.35	−6.44	14039	59,232	94	–
MI(AZ)-49-2	MaloInzer	617.5	0.46	0.85	−5.86	14824	59,379	90	–
MI(AZ)-57	MaloInzer	643.5	0.48	1.30	−8.36	7115	17,026	87	–
MI(AZ)-60	MaloInzer	646.5	0.49	0.72	−8.85	7923	42,923	86	–
MI(AZ)-63*	MaloInzer	649.5	0.02	−4.08	−13.40	2577	7865	63	–
MI(AZ)-72	MaloInzer	658.5	0.49	0.34	−9.53	8555	55,530	146	–
RV(AZ)-0-1	Revet	970.5	0.54	−1.28	−4.87	3709	26,734	194	–
RV(AZ)-0-3	Revet	970.5	0.55	−2.27	−9.13	4002	35,919	623	–
RV(AZ)-6-1	Revet	976.5	0.58	−1.04	−6.96	2047	19,193	302	–
RV(AZ)-6-1	Revet	976.5	0.58	−0.74	−6.64	2047	19,193	302	–
RV(AZ)-6-2	Revet	976.5	0.54	−1.15	−7.15	2082	17,301	198	–
RV(AZ)-11	Revet	981.5	0.57	−0.26	−6.66	1523	18,631	127	–
RV(AZ)-15	Revet	985.5	0.55	0.50	−6.56	1265	21,126	110	–
RV(AZ)-19.5-1	Revet	990.0	0.58	0.71	−6.27	1085	19,931	83	–
RV(AZ)-19.5-2	Revet	990.0	0.55	0.44	−5.79	1097	14,587	67	–
RV(AZ)-19.5-3	Revet	990.0	0.56	2.63	−13.36	1091	16,921	76	–
RV(AZ)-24	Revet	994.5	0.56	1.69	−4.54	850	8621	35	–
RV(AZ)-28.5	Revet	999.0	0.57	1.94	−3.82	849	5275	26	–
RV(AZ)-33	Revet	1003.5	0.57	1.99	−4.89	1203	9874	49	–
RV(AZ)-39.5-1	Revet	1010.0	0.56	2.40	−3.74	1391	11,582	67	–
RV(AZ)-39.5-2A	Revet	1010.0	0.56	2.06	−5.00	1354	11,621	64	–
RV(AZ)-39.5-2B	Revet	1010.0	0.57	2.32	−3.12	1382	10,136	61	–
RV(AZ)-44-1	Revet	1014.5	0.59	1.78	−4.12	887	4664	46	–
RV(AZ)-44-2	Revet	1014.5	0.60	1.73	−4.53	873	4565	48	–
RV(AZ)-51-1	Revet	1022.5	0.60	1.66	−5.25	267	2245	49	–
RV(AZ)-51-2A	Revet	1022.5	0.59	0.73	−5.94	449	2054	43	–
RV(AZ)-51-2B	Revet	1022.5	0.59	1.56	−7.70	422	8652	41	–
RV(AZ)-55.5-1	Revet	1027.0	0.57	1.62	−4.97	225	1729	58	–
RV(AZ)-55.5-2	Revet	1027.0	0.58	1.17	−5.70	462	2020	67	–
RV(AZ)-55.5-3	Revet	1027.0	0.58	1.43	−6.78	293	2461	111	–
RV(AZ)-55.5-3	Revet	1027.0	0.58	1.39	−6.89	293	2461	111	–
RV(AZ)-55.5-4	Revet	1027.0	0.59	1.00	−5.26	327	1877	90	–
RV(AZ)-60-1	Revet	1031.5	0.59	1.73	−4.94	266	1896	44	–
RV(AZ)-60-3	Revet	1031.5	0.57	1.55	−7.33	398	8653	37	–
RV(AZ)-68-1	Revet	1039.5	0.59	1.46	−4.51	230	1908	60	–
RV(AZ)-68-3	Revet	1039.5	0.57	1.58	−7.22	406	8223	22	–
RV(AZ)-70.5	Revet	1042.0	0.60	1.55	−3.49	342	2416	48	–
RV(AZ)-85.5	Revet	1057.0	–	1.29	−4.09	–	–	–	–
RV(AZ)-90-1	Revet	1061.5	0.58	1.55	−3.06	355	7493	59	–
RV(AZ)-90-2	Revet	1061.5	0.59	1.38	−5.90	198	3185	36	–
RV(AZ)-94.5	Revet	1066.0	0.60	2.15	−3.44	265	3635	56	–
RV(AZ)-100.5	Revet	1072.0	0.58	2.14	−3.06	371	2110	28	–
RV(AZ)-105-1	Revet	1076.5	0.59	2.24	−3.95	139	833	40	–
RV(AZ)-105-2	Revet	1076.5	0.58	2.02	−4.29	312	988	46	–
RV(AZ)-105-3	Revet	1076.5	0.58	1.95	−6.13	191	2746	109	–
RV(AZ)-105-3	Revet	1076.5	0.58	2.07	−6.33	191	2746	109	–
RV(AZ)-109.5	Revet	1081.0	0.59	2.39	−4.31	223	2063	30	–

Table 1 (*continued*)

Sample‡	Member	Height‡‡ (m)	Mg/Ca (w/w)	$\delta^{13}C$ (‰ VPDB)	$\delta^{18}O$ (‰ VPDB)	Mn (ppm)	Fe (ppm)	Sr (ppm)	$^{87}Sr/^{86}Sr$
RV(AZ)-114	Revet	1085.5	0.59	2.13	−1.42	131	2590	62	0.71531
RV(AZ)-118.5-1	Revet	1090.0	0.58	2.24	−2.17	195	1793	41	–
RV(AZ)-118.5-1	Revet	1090.0	0.58	1.95	−2.39	195	1793	41	–
RV(AZ)-118.5-2	Revet	1090.0	0.58	2.20	−2.27	211	2106	41	–
RV(AZ)-126	Revet	1097.5	0.58	1.74	−2.59	232	1617	42	–
RV(AZ)-127-1	Revet	1098.5	0.57	1.76	−3.19	279	8352	53	–
RV(AZ)-127-2A	Revet	1098.5	0.59	1.76	−2.85	277	8412	54	–
RV(AZ)-127-2B	Revet	1098.5	0.59	1.95	−2.81	272	8787	56	–
RV(AZ)-131.5-1	Revet	1106.0	0.56	1.75	−3.10	280	7418	57	–
RV(AZ)-131.5-2	Revet	1106.0	0.57	1.58	−2.84	319	6492	55	–
RV(AZ)-137-1	Revet	1111.5	0.45	2.07	−2.59	185	5529	68	–
RV(AZ)-137-2	Revet	1111.5	–	2.01	−2.53	–	–	–	–
RV(AZ)-142.5-1	Revet	1117.0	0.58	2.00	−2.36	184	2980	57	–
RV(AZ)-142.5-2	Revet	1117.0	–	1.93	−3.78	–	–	–	–
RV(AZ)-167.5	Revet	1142.0	0.58	0.94	−3.66	246	2462	58	–
RV(AZ)-174	Revet	1147.9	0.57	0.75	−3.58	265	3110	57	–
RV(AZ)-180	Revet	1153.9	0.59	1.63	−4.00	676	2135	48	–
RV(AZ)-186	Revet	1159.9	0.60	2.72	−5.60	292	1665	36	–
RV(AZ)-186	Revet	1159.9	0.60	2.83	−5.36	292	1665	36	–
RV(AZ)-192	Revet	1165.9	–	1.87	−4.47	–	–	–	–
RV(AZ)-198	Revet	1171.9	0.59	1.64	−3.23	257	1763	60	0.71140
RV(AZ)-204	Revet	1177.9	0.58	1.78	−2.67	198	1594	56	–
RV(AZ)-208.5	Revet	1182.4	0.60	1.92	−2.76	233	2651	77	–
RV(AZ)-214.5-1	Revet	1188.4	0.59	1.66	−2.91	258	3144	65	–
RV(AZ)-214.5-2	Revet	1188.4	0.61	1.77	−3.63	286	4059	61	–

‡Subsamples of individual phases are indicated by −1, −2, −3, −4 following sample number. Primary and early phases (marine cement, matrix, and clasts) are indicated by −1 or −2. Late-stage phases are indicated by −3 or −4. Late-stage phases are not included on chemostratigraphic curve (Fig. 9), but are included in figures addressing diagenesis.

‡‡Height measured in local continuous stratigraphic successions; adjusted to composite reference section.

Trace element content also provides a powerful tool for assessing degree of diagenesis. Sr, Mn, and Fe exhibit predictable behavior during alteration (Banner and Hanson, 1990). In general, Sr content decreases through interaction with relatively Sr-poor fluids. Examination of Sr content in Avzyan carbonates, however, shows a strong relationship with mineralogy and hence with $\delta^{18}O$ (Fig. 5), suggesting that the principal control on Sr content is mineralogy. Sr is systematically excluded from the tighter dolomite lattice structure during dolomitization, resulting in dolostones with lower Sr content than coeval limestone. Initial Sr concentration disparity between limestone and dolostone is preserved, even through later water–rock interactions, as evidenced by scatter in $\delta^{18}O$ values and the poor preservation of Sr-isotopic signatures. Limestones and dolostones must therefore be considered separately when evaluating the Sr diagenetic history of these rocks.

Mn content typically increases with water–rock interaction in the presence of reduced fluids and therefore generally reflects either carbonate precipitation in the presence of Mn-rich waters (as might be expected in microbial mats), or post-depositional alteration under burial conditions. As with Sr, Mn shows distinctly different trends for limestone and dolostone in the Avzyan Formation (Fig. 6A). For each phase, Mn increases toward lower $\delta^{18}O$ values, consistent with

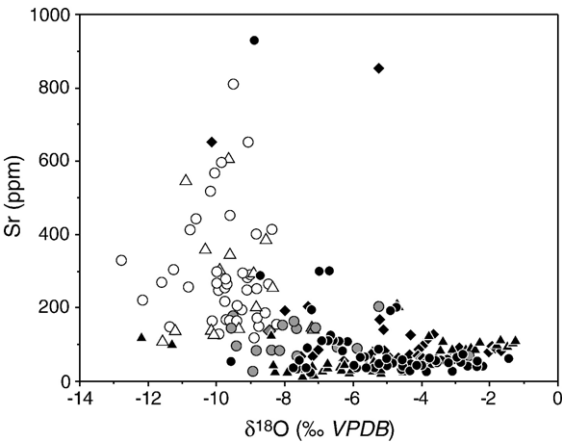

Fig. 5. Mineralogical partitioning as recorded in strontium concentration of Avzyan Formation carbonates. Elevated Sr concentrations (>100 ppm) occur predominantly in limestones (open symbols), whereas lower Sr concentrations (<200 ppm) occur in calcic dolostone (grey symbols) and dolostone lithologies (black symbols), suggesting that lattice structure is the primary control on Sr concentration. Legend provided in Fig. 4.

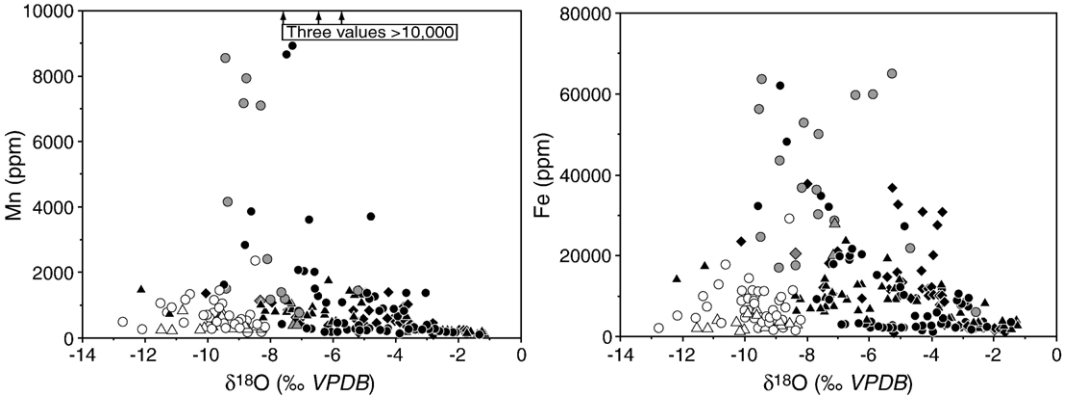

Fig. 6. Manganese and iron concentrations of Avzyan Formation carbonates, plotted against oxygen isotope composition. All lithologies show similar range of Mn and Fe with the majority of data recording values <2000 ppm for Mn and <15,000 ppm for Fe. These concentrations are significantly elevated over most well-preserved Mesoproterozoic to Neoproterozoic aged carbonates (cf. Kah et al., 1999b; Frank and Lyons, 2000; Kah, 2000; Bartley et al., 2001; Frank et al., 2003; Kah et al., 2004), yet show no distinct diagenetic trends within these concentration limits. With the exception of dolomite samples from the Katav River locality (black diamonds) and a single limestone sample from the Avzyan locality (white circle), samples with Mn >2000 ppm and Fe >15 000 ppm are comprised predominantly of dolostones and calcic dolostones with the depleted oxygen isotope compositions and secondary phases (crosscutting veins, late-stage void fills), which supports an interpretation of overprinting by late-stage diagenetic fluids. Legend provided in Fig. 4.

the expected diagenetic trend (Banner and Hanson, 1990). Dolostones contain more Mn on average than limestones, likely reflecting a combination of increased Mn mobility associated with microbial activity in peritidal environments and diagenesis by later fluids.

The relationships of Fe content to mineralogy and $\delta^{18}O$ values are broadly similar to those observed for Mn (Fig. 6B). Limestone and dolostone samples show distinctly different trends with respect to iron content, again suggesting that samples retain different initial iron concentrations. Dolostone samples, on average, contain more Fe than do limestones, and samples with intermediate Mg/Ca ratios have the highest Fe contents, suggesting more extensive water–rock interaction in these samples.

Assessment of Mn and Fe behavior in the context of mineralogy and fabric preservation is particularly useful. For limestone and dolostone samples with fine-scale fabric preservation, Mn and Fe contents are relatively low. Poor fabric preservation, typical of samples with intermediate Mg/Ca, is associated with marked enrichment in both Mn and Fe (Fig. 7). Examining the relationship between Mn and Fe content in samples of the Avzyan reveals a cluster of samples with lower Mn and Fe concentrations, and a spread of points with Mn>500 ppm and/or Fe>12,000 ppm, suggestive of significant alteration. Furthermore, where individual diagenetic phases are present, late-stage elements (veins and sparry cement; sample numbers designated −3 or −4 in Tables 1–3) confirm these trends within individual hand samples.

In carbonates such as these, which have experienced moderate to severe post-depositional alteration, there is no clear cohort of samples that are “little altered” or “unaltered” (cf. Frank and Lyons, 2000) that would provide a set of geochemical criteria for accepting or rejecting carbon isotopic data. The Mn and Fe values identified above are an order of magnitude higher than those considered little-altered by other authors (Kaufman and Knoll, 1995; Frank and Lyons, 2000; Bartley et al., 2001). Instead, most samples possess broadly similar diagenetic characteristics, and a few show evidence of pervasive alteration. Even against such a

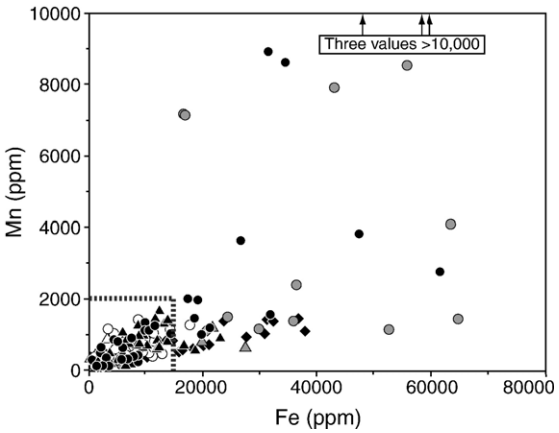

Fig. 7. Mn and Fe concentrations of Avzyan carbonates, illustrating concentration limits (Mn <2000 ppm and Fe <15000 ppm) taken to represent best-preserved samples. Legend provided in Fig. 4.

Table 2
Isotopic and elemental compositions, Avzyan Formation carbonates (Kataskin Locality)

Sample‡	Member	Height‡‡ (m)	Mg/Ca (w/w)	$\delta^{13}C$ (‰ VPDB)	$\delta^{18}O$ (‰ VPDB)	Mn (ppm)	Fe (ppm)	Sr (ppm)
KT(KT)-20	Kataskin	80.0	0.59	0.63	−6.33	846	6154	31
KT(KT)-32	Kataskin	92.0	0.58	0.64	−7.47	1090	5889	29
KT(KT)-47	Kataskin	107.0	0.57	0.50	−7.14	786	7069	16
KT(KT)-57	Kataskin	117.0	0.57	0.71	−7.90	800	6458	24
KT(KT)-63	Kataskin	123.0	0.58	0.18	−6.01	540	6078	32
KT(KT)-67.5	Kataskin	127.5	0.59	0.54	−7.17	742	10,283	40
KT(KT)-97−1	Kataskin	157.0	0.58	0.75	−6.73	751	8551	37
KT(KT)-97-2	Kataskin	157.0	0.53	0.36	−8.39	1027	9763	124
KT(KT)-120*	Kataskin	180.0	0.54	−1.81	−5.15	732	15,976	115
KT(RR)-0	Kataskin	80.0	0.54	0.60	−6.56	1083	8536	28
KT(RR)-6	Kataskin	86.0	0.53	0.72	−6.87	681	9801	29
KT(RR)-9-1	Kataskin	89.0	0.59	1.01	−6.09	502	3646	23
KT(RR)-9-3	Kataskin	89.0	0.59	0.68	−7.41	1020	8806	22
KT(RR)-13-1	Kataskin	93.0	0.60	0.63	−7.54	764	6353	33
KT(RR)-13-2	Kataskin	93.0	0.61	0.81	−7.39	878	6910	30
KT(RR)-18	Kataskin	98.0	0.59	0.65	−4.49	839	8157	27
KT(RR)-24-1*	Kataskin	104.0	0.57	0.20	−7.56	781	8689	26
KT(RR)-24-3	Kataskin	104.0	0.55	0.27	−9.92	1288	17,353	111
KT(RR)-36-1	Kataskin	116.0	0.57	−0.31	−7.38	908	12,085	33
KT(RR)-36-3	Kataskin	116.0	–	−0.27	−7.58	–	–	–
KT(RR)-36-4	Kataskin	116.0	–	−0.50	−6.85	–	–	–
KT(RR)-41-1	Kataskin	121.0	0.01	0.40	−10.15	317	755	139
KT(RR)-41-2	Kataskin	121.0	0.01	−0.34	−11.19	260	1544	137
KT(RR)-41-3	Kataskin	121.0	0.00	0.56	−10.02	392	1197	128
KT(RR)-50	Kataskin	130.0	0.54	0.76	−6.75	962	23,176	45
KT(RR)-56	Kataskin	136.0	0.55	0.66	−6.37	711	12,240	35
KT(RR)-75	Kataskin	155.0	0.01	0.69	−9.32	275	1879	143
KT(RR)-78-1	Kataskin	158.0	0.37	1.61	−7.12	698	27,417	147
KT(RR)-78-3	Kataskin	158.0	–	1.66	−7.57	–	–	–
KT(RR)-90	Kataskin	170.0	0.01	1.45	−8.82	297	2601	200
KT(RR)-106	Kataskin	186.0	0.01	0.95	−11.56	286	1902	108
AZ(IZ)-0	Kataskin	433.0	0.58	2.46	−8.24	823	8916	24
AZ(IZ)-50	Kataskin	438.0	0.57	2.48	−8.31	614	5914	43
AZ(IZ)-238	Kataskin	456.8	0.02	2.12	−8.33	314	2263	258
AZ(IZ)-250-1	Kataskin	458.0	0.03	2.51	−8.52	331	2732	386
AZ(IZ)-250-2	Kataskin	458.0	0.33	3.05	−7.15	869	19,603	140
AZ(IZ)-300	Kataskin	463.0	0.02	1.89	−8.90	396	3145	297
AZ(IZ)-348-1	Kataskin	467.8	0.02	2.49	−9.60	672	4907	605
AZ(IZ)-348-2*	Kataskin	467.8	0.02	2.86	−8.88	629	5196	71
AZ(IZ)-349	Kataskin	467.9	0.02	2.67	−9.59	768	6098	348
AZ(IZ)-450	Kataskin	478.0	0.58	3.80	−7.45	908	13,617	11
AZ(IZ)-540	Kataskin	487.0	0.03	3.14	−9.91	378	5100	306
AZ(IZ)-554	Kataskin	488.4	0.02	3.27	−10.29	269	3158	359
AZ(IZ)-600*	Kataskin	493.0	0.18	0.31	−4.71	1243	21,360	205
AZ(IZ)-610	Kataskin	494.0	0.01	2.87	−10.88	861	3522	545
AZ(KT)-0	Ushakov	800.5	0.53	2.25	−5.04	1360	13,395	40
AZ(KT)-6	Ushakov	806.5	0.55	2.49	−5.17	1341	11,147	23
KT(KT)-12.5-1	Ushakov	813.0	0.54	2.19	−6.24	1758	12,288	44
KT(KT)-12.5-2	Ushakov	813.0	0.52	2.02	−12.19	1453	13,778	117
AZ(KT)-18	Ushakov	818.5	0.55	2.54	−5.59	1469	11,622	45
AZ(KT)-23	Ushakov	823.5	0.56	2.37	−5.40	1325	8694	30
RV(KT)-0-1	Revet	905.5	0.59	1.17	−5.39	644	18,789	56
RV(KT)-0-2	Revet	905.5	0.60	1.36	−3.70	635	12,071	45
RV(KT)-0-3	Revet	905.5	0.50	0.96	−11.29	753	16,897	102
RV(KT)-24-1	Revet	929.5	0.60	2.23	−1.25	111	1953	111
RV(KT)-24-2A	Revet	929.5	0.60	1.85	−3.75	200	6537	124
RV(KT)-24-2B	Revet	929.5	0.61	–	–	165	2278	97

(continued on next page)

Table 2 (*continued*)

Sample‡	Member	Height‡‡ (m)	Mg/Ca (w/w)	$\delta^{13}C$ (‰ VPDB)	$\delta^{18}O$ (‰ VPDB)	Mn (ppm)	Fe (ppm)	Sr (ppm)
RV(KT)-31	Revet	936.5	0.62	0.57	−3.38	196	3920	108
RV(KT)-37-1	Revet	942.5	0.60	2.70	−1.46	134	1384	95
RV(KT)-37-3	Revet	942.5	0.60	–	–	139	1663	104
RV(KT)-42-1	Revet	947.5	0.61	−0.59	−1.31	174	3454	107
RV(KT)-42-2	Revet	947.5	0.58	−0.52	−1.67	199	2148	111
RV(KT)-49-1	Revet	954.5	0.62	0.34	−1.76	164	2979	99
RV(KT)-49-2	Revet	954.5	0.60	–	–	192	2816	106
RV(KT)-55-1	Revet	960.5	0.61	0.10	−2.28	225	7673	107
RV(KT)-55-2	Revet	960.5	0.61	−0.09	−2.53	232	1546	93
RV(KT)-60-1	Revet	965.5	0.61	−1.80	−2.41	245	2638	87
RV(KT)-60-3	Revet	965.5	0.61	−1.82	−2.48	246	2906	89
RV(KT)-65-1	Revet	970.5	0.58	−1.08	−3.42	267	3903	83
RV(KT)-65-3	Revet	970.5	0.59	−1.03	−3.42	342	5261	86
RV(KT)-70-1	Revet	975.5	0.62	−1.26	−2.68	226	2905	86
RV(KT)-70-2	Revet	975.5	0.61	–	–	227	4094	91

‡Subsamples of individual phases are indicated by −1, −2, −3 following sample number. Primary and early phases (marine cement, matrix, and clasts) are indicated by −1 or −2. Late-stage phases are indicated by −3. Late-stage phases are not included on chemostratigraphic curve (Fig. 9), but are included in figures addressing diagenesis.

‡‡Height measured in continuous stratigraphic succession; adjusted to composite reference section.

background of moderate diagenesis, we expect that the fundamental character of a carbon isotopic curve might be retained. Significant covariance between $\delta^{13}C$ and any of the diagenetic indicators would suggest systematic alteration of carbon isotopic composition with diagenesis. Such a trend is not observed in Avzyan samples (Fig. 8). Carbon isotopic composition is unrelated to mineralogy, Mn content (Fig. 8A), or Fe content (Fig. 8B), indicating that no carbon isotopic data should be rejected based on standard diagenetic criteria. In other words, these standard diagenetic criteria do not explain the observed variance in $\delta^{13}C$, and thus are unsuitable for distinguishing "well-preserved" $\delta^{13}C$ values from "poorly-preserved" values.

In order to determine whether observed carbon isotopic compositions are likely to record a secular pattern of carbon isotopic change, we use other tools at our disposal. Numerous carbon isotopic studies have shown that stratigraphic $\delta^{13}C$ patterns are retained even with significant diagenesis (Fairchild et al., 1990; Kaufman et al., 1991; Frank and Lyons, 2000). A stratigraphic pattern of carbon isotopic change is a strong indicator of a robust signal, particularly if the pattern is expressed by numerous samples from different localities and with different mineralogic, textural and geochemical characteristics (Kaufman and Knoll, 1995). Secondly, preservation of a stratigraphic pattern in $\delta^{13}C$ of organic matter as well as carbonate carbon argues in favor of a pattern of depositional, rather than diagenetic variation (Kaufman et al., 1991). Although processes are known that affect both $\delta^{13}C_{carb}$ and $\delta^{13}C_{org}$, none is known that affects both organic and inorganic carbon isotopic values at the same rate and in the same direction. For example, meteoric diagenesis typically causes $\delta^{13}C_{carb}$ to decrease, while $\delta^{13}C_{org}$ remains largely unaffected (Kaufman et al., 1991). In contrast, thermal alteration generally causes loss of ^{12}C from organic carbon, resulting in an increase in $\delta^{13}C_{org}$ (Strauss et al., 1992). If $\delta^{13}C_{carb}$ is affected by thermal alteration, it typically incorporates ^{12}C lost from organic carbon, resulting in a decrease in the $\delta^{13}C$ composition of carbonate. In both processes, the net result is that $\Delta\delta$ ($\delta^{13}C_{carb} - \delta^{13}C_{org}$) decreases, and the amount of the decrease depends strongly upon the relative concentrations of C_{org} and C_{carb}. Thus, a consistent difference between $\delta^{13}C_{org}$ and $\delta^{13}C_{carb}$, particularly across facies boundaries, suggests little alteration of $\delta^{13}C$ values. In the Kataskin Member, $\delta^{13}C_{org}$ values obtained from shales interbedded with sampled carbonates showed a consistent offset of −23‰. Consistent $\Delta\delta$ values as well as persistent stratigraphic $\delta^{13}C$ patterns throughout the Avzyan Formation strongly suggest that change through time, locally or globally, is the likely cause of carbon isotopic variability in the Avzyan Formation.

4.2. Chemostratigraphy

The carbon isotope chemostratigraphy of the Avzyan Formation (Fig. 9) is broadly similar to patterns observed in other Mesoproterozoic carbonate successions. The lower portion of the Kataskin Member preserves $\delta^{13}C$ values mainly between 0 and +1‰, with a maximum of +1.7‰. The upper Kataskin exhibits an overall rise in $\delta^{13}C$ to values typically between +1.5 and

Table 3
Isotopic and elemental compositions, Avzyan Formation carbonates (Katav River Locality)

Sample‡	Member	Height‡‡ (m)	Mg/Ca (w/w)	$\delta^{13}C$ (‰ VPDB)	$\delta^{18}O$ (‰ VPDB)	Mn (ppm)	Fe (ppm)	Sr (ppm)
(AV)SL16.1-1	Ushakov	0.5	0.60	1.08	−4.08	853	11,542	74
(AV)SL16.1-2	Ushakov	0.5	0.61	0.82	−5.44	870	14,427	80
(AV)SL16.2-1	Ushakov	5.5	0.60	0.89	−7.50	857	11,873	71
(AV)SL16.2-2	Ushakov	5.5	0.60	0.61	−4.95	868	13,132	68
(AV)SL16.2-3	Ushakov	5.5	0.44	−0.61	−8.40	1145	20,388	140
(AV)SL16.3	Ushakov	10.5	0.59	1.00	−4.09	651	9968	91
(AV)SL16.4	Ushakov	12.5	0.58	1.53	−5.38	649	11,076	83
(AV)SL17.5-1	Ushakov	2.5	0.57	0.60	−5.09	577	15,611	144
(AV)SL17.5-3	Ushakov	2.5	0.57	0.27	−7.30	649	17,874	208
(AV)SL17.6-1	Ushakov	7.5	0.56	0.81	−3.97	703	19,744	67
(AV)SL17.6-3	Ushakov	7.5	0.58	0.20	−7.02	713	20,747	90
(AV)SL17.7	Ushakov	12.5	0.57	0.62	−4.32	603	16,056	129
(AV)SL17.8	Ushakov	19.5	0.56	−0.13	−3.82	979	27,104	119
(AV)SL17.9-1	Ushakov	22.5	0.56	−0.06	−3.65	1038	30,409	130
(AV)SL17.9-3	Ushakov	22.5	0.54	−0.48	−8.00	1123	37,565	194
(AV)SL17.10-1	Ushakov	29.5	0.55	0.44	−4.33	1413	30,779	74
(AV)SL17.10-3	Ushakov	29.5	0.55	−0.28	−10.12	1405	23,373	656
(AV)SL17.11-1	Ushakov	32.5	0.56	0.14	−5.07	1402	32,130	86
(AV)SL17.11-3	Ushakov	32.5	0.55	−0.33	−5.23	1473	36,219	855
(AV)SL21.13	Revet	5.5	0.58	0.67	−3.67	459	9810	61
(AV)SL21.14-1	Revet	10.5	0.60	0.59	−3.77	543	10,203	59
(AV)SL21.14-2	Revet	10.5	0.60	0.70	−4.12	637	11,708	52
(AV)SL21.15-1	Revet	15.5	0.59	0.53	−4.02	558	11,916	66
(AV)SL21.15-2	Revet	15.5	0.60	0.71	−4.31	647	11,536	50
(AV)SL21.16-1	Revet	20.5	0.58	0.89	−3.74	371	7525	62
(AV)SL21.16-2A	Revet	20.5	0.60	0.87	−4.11	522	9547	49
(AV)SL21.16-2B	Revet	20.5	0.60	0.88	−3.60	433	8042	59
(AV)SL22.17-1	Revet	0.0	0.59	0.76	−3.95	464	9213	65
(AV)SL22.17-2	Revet	0.0	0.59	0.82	−4.67	437	9147	61
(AV)SL22.17-3	Revet	0.0	0.54	0.41	−6.26	491	10,421	72
(AV)SL22.17-4	Revet	0.0	0.57	0.35	−7.17	509	9835	102
(AV)SL22.19	Revet	5.0	0.61	1.82	−3.12	350	2324	64
(AV)SL22.19-2	Revet	10.0	0.60	1.67	−2.03	266	1223	82
(AV)SL22.19-1A	Revet	10.0	0.60	1.80	−1.68	216	696	85
(AV)SL22.19-1B	Revet	10.0	0.60	1.81	−3.56	350	2495	62
(AV)SL22.20-1	Revet	18.0	0.61	1.75	−2.57	245	2086	83
(AV)SL22.20-2A	Revet	18.0	0.61	1.54	−1.82	288	1482	94
(AV)SL22.20-2B	Revet	18.0	0.62	1.51	−1.93	271	1552	99
(AV)SL22.21-1A	Revet	23.0	0.61	2.30	−2.86	170	1796	96
(AV)SL22.21-2	Revet	23.0	0.60	1.32	−1.85	147	1431	93
(AV)SL22.21-3	Revet	23.0	0.61	1.49	−1.88	284	1555	94
(AV)SL22.22-1	Revet	28.0	0.61	1.32	−5.05	406	9868	48
(AV)SL22.22-2	Revet	28.0	0.60	1.74	−2.86	484	2366	80
(AV)SL22.22-3	Revet	28.0	0.61	1.91	−5.23	180	427	171
(AV)SL22.23	Revet	29.5	0.61	1.32	−2.00	287	1682	87

‡Subsamples of individual phases are indicated by −1, −2, −3, −4 following sample number. Primary and early phases (marine cement, matrix, and clasts) are indicated by −1 or −2. Late-stage phases are indicated by −3 or −4. Late-stage phases are not included on chemostratigraphic curve (Fig. 9), but are included in figures addressing diagenesis.
‡‡Local height from base of individual outcrops successions; structural dissection precludes calculation of total stratigraphic height.

+2‰, with $\delta^{13}C$ values between +3.0 and +4.5‰ recorded in the uppermost ~75 m of Kataskin strata as excursions above this moderately positive baseline. Carbon isotope values recorded in small bioherms in the upper half of the Malo Inzer Member cluster around +1‰, then rise to +2‰ in the upper Ushakov Member. No samples were analyzed from the siliciclastic Kutkur Member; however, samples from the base of the overlying Revet Member show a sharp drop from moderately positive values between +1.0 and +2.7‰, similar to those recorded in the upper Ushakov member, to values of −2‰, followed by a sharp rise to +2.3‰,

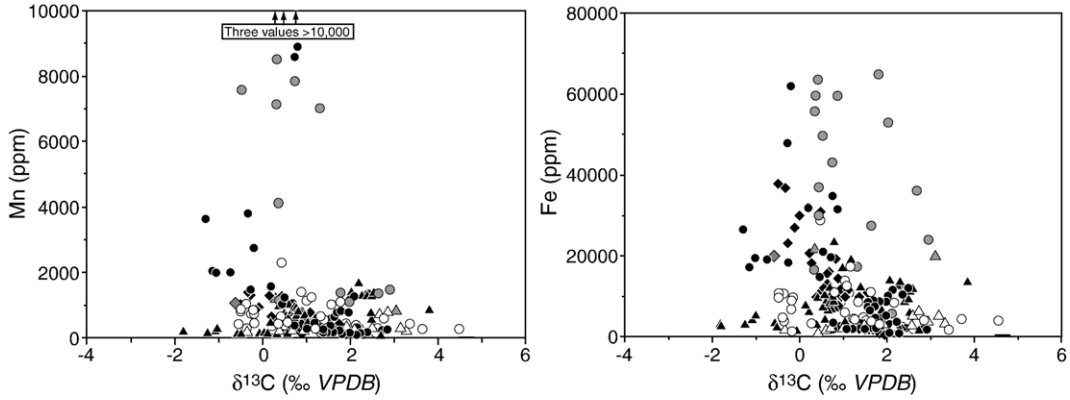

Fig. 8. Manganese and iron concentrations of Avzyan Formation carbonates, plotted against carbon isotopic composition. Within concentration limits taken to represent best-preserved samples (see Figs. 6 and 7), there is no distinct relationship between Mn and Fe concentration and carbon isotope composition, suggesting that post depositional alteration had no systematic effect on carbon isotopes. Legend provided in Fig. 4.

followed by more steady carbon isotope signatures near +2‰ for the remainder of Revet deposition.

Although precise stratigraphic positioning is uncertain for samples analyzed from the Ushakov and Revet members at the Katav River locality, Revet samples show a rapid rise from values near +0.4‰ to values exceeding +2‰ (Table 3), which is consistent with depositional signatures from the lower Revet at Avzyan. Ushakov samples collected from the structurally complex and stratigraphically dissected Katav locality show values predominantly between −0.5‰ and +0.5‰ near the base of exposed Ushakov strata, rising to values as high as +1.5‰ at higher stratigraphic levels. These values are unlike those recorded from both the underlying Malo Inzer member and the uppermost Ushakov strata sampled near Inzer, suggesting the presence of a short-lived negative excursion in lower Ushakov strata. Lower Ushakov strata are present at Inzer, but accessible only when water levels in the Malo Inzer River are low.

Organic carbon analyses from interbedded, organic rich (TOC 0.1 to 2.8%; average 1%) shales of the Zigazino–Komorovo Formation and Kataskin Member provide an additional measure of marine carbon isotopic change during lower Avzyan deposition (Fig. 9). Organic carbon analyses reveal values between −25.1‰ and −26.6‰ in the uppermost Zigazino–Komorovo Formation. In the Kataskin Member, $\delta^{13}C_{org}$ values rise from approximately −24‰ in the lower Kataskin to values predominantly between −21‰ and −23‰ in the upper Kataskin, with a few heavier values, to −18‰, in the upper 100 m of the Kataskin Member, in relatively organic-poor samples (Table 4). The isotopic pattern preserved in Kataskin organic matter parallels that observed in carbonate, indicating that observed stratigraphic variability in $\delta^{13}C$ reflects secular change, rather than carbonate diagenesis. Utilizing the average difference between the isotopic compositions of adjacent carbonate and shale beds in the Kataskin Member, we arrive at an estimated 23‰ isotopic difference ($\Delta\delta C$) associated with microbial DIC reduction and organic matter preservation.

Application of this 23‰ $\Delta\delta C$ to Zigazino–Komorovo shales suggests DIC isotopic values near −3‰. Because the Zigazino–Komarovo Formation preserves no carbonate, it is impossible to determine whether these relatively light values indicate secular variation in seawater carbonate composition or reflect significantly different depositional and/or diagenetic conditions for Zigazino–Komarovo organic material, such as a deeper-water environment influenced by anoxia or rapid decomposition of organic material.

5. Discussion

Despite the fact that rocks of the Avzyan Formation have experienced moderate to severe regional alteration, a consistent pattern of variation in carbon isotopic composition is observed. The C-isotope chemostratigraphy of the Avzyan Formation is broadly similar to other Mesoproterozoic successions younger than ~1300 Ma and older than ~1250 Ma, with moderately positive $\delta^{13}C$ values that become increasingly positive upward, rising from ~0‰ to ~+2‰.

In order to better constrain the position of the Avzyan Formation within the emerging Mesoproterozoic carbon isotopic framework, we must examine the isotopic characteristics of the known portions of the global curve. Isotopic evolution of the Mesoproterozoic, as recorded in carbonates and coeval organic matter, can be

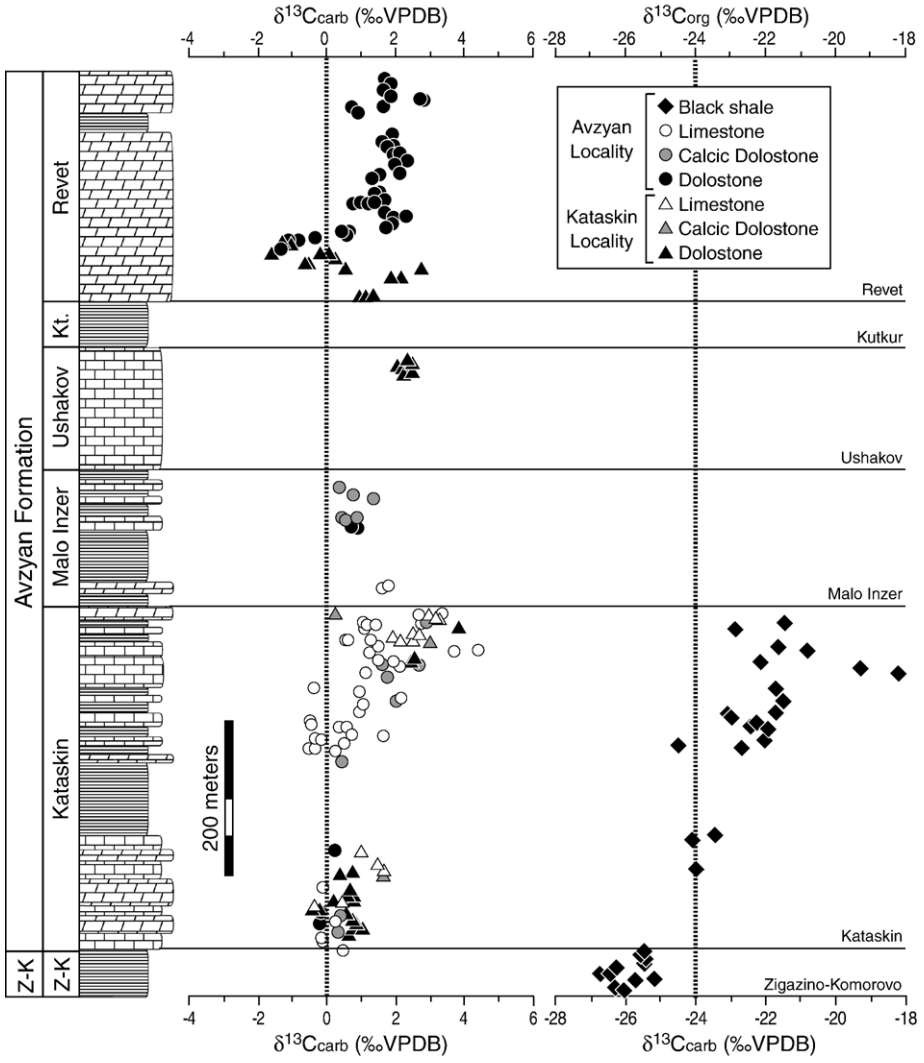

Fig. 9. Stratigraphic variation in carbon isotope composition of carbonates from the Avzyan Formation (Avzyan and Kataskin localities) and organic carbon from black shales from the Zigazino–Komorovo and Avzyan formations (Avzyan locality). Where both carbonate and organic carbon samples were available, isotopic compositions track with 24‰ offset. Combined, these values preserve a pattern of moderate isotopic variability, wherein marine DIC is inferred to have varied between approximately −2‰ and +2‰. Stratigraphic patterns preserved here are broadly similar to those preserved in 1300 Ma–1270 Ma strata of the Dismal Lakes Group (Frank et al., 2003), suggesting preservation of a global carbon isotope signal. A short interval of more positive carbon isotope values (to +4‰) near the top of the Kataskin Member, Avzyan Formation, are unknown from other successions of this age (*see discussion in text*).

subdivided into two primary intervals, characterized by differences in both average $\delta^{13}C$ and in the magnitude of observed isotopic excursions. The pre-1300 Ma global C isotope record has $\delta^{13}C$ values near 0‰ with excursions <2‰ (Buick et al., 1995; Knoll et al., 1995; Frank et al., 1997; Xiao et al., 1997; Lindsay and Brasier, 2000). Mesoproterozoic strata from the Kaltasin Formation of the East European Platform have $\delta^{13}C$ values near 0‰. These strata have been correlated with the Lower Riphean Bakal Formation of the Southern Urals (Keller and Chumakov, 1983; Maslov, 1994), which is constrained to be >1360 Ma (Ellmies et al., 2000). This interval of isotopic stasis persists until at least 1305 Ma, as recorded in carbonates in the Uchur–Maya region of Siberia that overlie siliciclastic rocks containing 1305 Ma detrital zircons (Rainbird et al., 1998; Bartley et al., 2001).

In contrast, Late Mesoproterozoic carbonates, including successions from western Siberia (Knoll et al., 1995; Bartley et al., 2001), eastern Siberia (Bartley et al.,

Table 4
Isotopic composition, Avzyan Formation shales (Avzyan locality)

Sample	Member	Height‡ (m)	$\delta^{13}C_{org}$ (‰ VPDB)
ZK(AZ)-8	Zigazino–Komorovo	8.0	−25.93
ZK(AZ)-12	Zigazino–Komorovo	12.0	−26.23
ZK(AZ)-18.5	Zigazino–Komorovo	18.5	−25.58
ZK(AZ)-21.7	Zigazino–Komorovo	21.7	−25.07
ZK(AZ)-26	Zigazino–Komorovo	26.0	−26.59
ZK(AZ)-30.4	Zigazino–Komorovo	30.4	−26.28
ZK(AZ)-35.8	Zigazino–Komorovo	35.8	−26.16
ZK(AZ)-42.4	Zigazino–Komorovo	42.4	−25.28
ZK(AZ)-47	Zigazino–Komorovo	47.0	−25.36
ZK(AZ)-52.4	Zigazino–Komorovo	52.4	−25.42
ZK(AZ)-58	Zigazino–Komorovo	58.0	−25.33
KT(AZ)-104	Kataskin	164.0	−23.85
KT(AZ)-142	Kataskin	202.0	−23.94
KT(AZ)-150	Kataskin	210.0	−23.29
KT(AZ)-221	Kataskin	324.0	−22.60
KT(AZ)-225.3	Kataskin	328.3	−24.37
KT(AZ)-231.1	Kataskin	334.0	−21.88
KT(AZ)-244.5	Kataskin	347.5	−21.76
KT(AZ)-248.5	Kataskin	351.5	−22.33
KT(AZ)-253.5	Kataskin	356.5	−22.14
KT(AZ)-259	Kataskin	362.0	−22.83
KT(AZ)-263.3	Kataskin	366.3	−22.94
KT(AZ)-268.8	Kataskin	371.8	−21.64
KT(AZ)-281.3	Kataskin	384.3	−21.37
KT(AZ)-297	Kataskin	400.0	−21.56
KT(AZ)-308	Kataskin	411.0	−26.55
KT(AZ)-316	Kataskin	419.0	−18.04
KT(AZ)-322.3	Kataskin	425.3	−19.16
KT(AZ)-333	Kataskin	436.0	−22.09
KT(AZ)-347	Kataskin	450.0	−20.63
KT(AZ)-352.5	Kataskin	455.5	−21.54
KT(AZ)-374	Kataskin	477.0	−22.76
KT(AZ)-384	Kataskin	487.0	−21.28

‡Height measured in continuous stratigraphic succession; adjusted to composite reference section.

2001), arctic Canada (Kah et al., 1999b, 2001), and west Africa (Fairchild et al., 1990) record positive $\delta^{13}C$ values (+3.5‰) with higher-amplitude (4‰–5‰) excursions (Knoll et al., 1995; Kah et al., 1999b; Bartley et al., 2001; Bartley and Kah, 2004). Carbon isotope compositions from the Allamoore Formation of west Texas (1250+16/−24 Ma; Roths, 1993) lie between +2 and +4‰ (Kah and Bartley, 1997), suggesting that moderately positive carbon isotope compositions had been attained by *ca.* 1250 Ma.

The Dismal Lakes Group, arctic Canada, which is constrained to be older than 1267±2 Ma (LeCheminant and Heaman, 1989) preserves low, positive $\delta^{13}C$ values between 0 and +2‰ (Frank et al., 2003), thus differentiating it from both older, less variable successions and younger, more positive and variable intervals. Thus, the emerging Mesoproterozoic carbon isotopic record provides a testable framework for broad geochronologic interpretations of successions of uncertain age. Carbonates older than ~1300 Ma will preserve $\delta^{13}C$ values near 0‰, with low variability. Successions younger than 1250 Ma contain $\delta^{13}C$ values near +3.5‰ with increased variation. The transitional interval between 1300 and 1250 Ma preserves chemostratigraphic profiles of intermediate character (0‰ to +2‰ with modest variability). Using these criteria, we should be able to place the Avzyan Formation into a global chemostratigraphic context.

The carbon isotope chemostratigraphy of the Avzyan Formation shows relatively low-magnitude isotopic change. Over the entire formation, $\delta^{13}C$ values increase from near 0‰ to +2‰ with excursions of moderate magnitude. This pattern is unlike those observed in late Mesoproterozoic successions (<1250 Ma) worldwide, in that the Avzyan lacks stable isotopic plateaus near +3‰. On the other hand, the chemostratigraphic profile, particularly that of the Revet Member, is strikingly similar to that observed in the well-preserved platform sediments of the Dismal Lakes Group (Frank et al., 2003). Both the Revet Member and the Dismal Lakes Group contain moderately positive $\delta^{13}C$ values with excursions up to a few permil. Unlike the Dismal Lakes Group, however, the top of the Kataskin Member preserves an excursion to more highly positive values, up to +4.5‰, suggesting that these two units cannot be correlated directly, but rather, represent broadly coeval depositional intervals. The observed similarity between the Avzyan Formation and Dismal Lakes Group suggests that the Avzyan Formation is younger than ~1300 Ma and older than ~1250 Ma, and forms part of the mid-Mesoproterozoic transition from low, invariant $\delta^{13}C$ values to positive, variable compositions. These age estimates are consistent with, but not uniquely constrained by, existing geochronologic data, which require the Avzyan Formation to be younger than 1360 Ma and older than 1080 Ma.

The presence of a distinctly positive interval at the top of the Kataskin member deserves special attention. Isotopic values above +3‰ are rare prior to ~1250 Ma, and typically occur within a framework of overall

positive $\delta^{13}C$ values. Three explanations are possible for the Avzyan Formation: 1) these values are an artifact of diagenesis; 2) these values are local, rather than global in nature; and 3) these values represent a potentially distinctive, global isotopic excursion. It is unlikely that diagenetic alteration is responsible for the strongly positive values of the Kataskin Member. First, diagenesis typically alters $\delta^{13}C$ toward more negative values. Second, the positive excursion appears as part of an overall stratigraphic trend toward elevated $\delta^{13}C$ values, rather than isolated samples against a low background. Third, $\delta^{13}C_{org}$ values also record a positive shift through this same interval. At this stage, it is impossible to discern whether the highly positive values are global or local in nature. If global, these distinctive values >+4‰ provide potentially diagnostic robust chemostratigraphic markers for future chemostratigraphic study, and might suggest the influence of pre-Grenvillian tectonic events on the Late Mesoproterozoic carbon cycle. If local, elevated $\delta^{13}C$ values may represent proximity to a major C_{org} depocenter, which would cause regional elevation of $\delta^{13}C$ (Frank et al., 2003).

Regardless of the precise geochronologic position of the Avzyan Formation, its carbon isotopic composition lends strength to earlier arguments regarding the nature of the mid-Mesoproterozoic isotopic shift. A shift from 0‰ to +3.5‰ corresponds to a 50% increase in the relative flux of organic carbon, based on steady-state model conditions (Frank et al., 2003). The intermediate nature of both Avzyan and Dismal Lakes $\delta^{13}C$ values suggests that the transition occurred over a relatively protracted time interval, rather than in a single event, and that the transitional interval itself is characterized by shorter-term fluctuations in $\delta^{13}C$. It is difficult to envision, however, how a 50% increase in organic carbon burial, derived simply from enhanced organic production, weathering, or orogeny, could be sustained for the several hundred million years of the latter Mesoproterozoic. In an alternative hypothesis, such a shift could represent a profound reorganization of the global carbon cycle driven ultimately by a secular decrease in marine DIC (Bartley and Kah, 2004). A secular decrease in marine DIC through the Mesoproterozoic would drive in an increased sensitivity of the marine system to natural variation in organic carbon burial fluxes, resulting in a gradual increase in the extent of isotopic variation recorded in marine systems. In addition to increased isotopic sensitivity, a secular decrease in marine DIC would lead to the spatial partitioning of organic and inorganic carbon burial, ultimately resulting in increased organic carbon sequestration (Bartley and Kah, 2004) and ocean-atmosphere oxygenation (Des Marais et al., 1992).

6. Conclusions

Carbon isotope chemostratigraphic data can be recoverable even in successions that have undergone considerable diagenesis that has overprinted other geochemical data, such as $\delta^{18}O$, $^{87}Sr/^{86}Sr$, Mn, Sr, and Fe. Geochemical tests can be used to evaluate the degree of diagenesis that rocks have undergone, but the high resistance of $\delta^{13}C$ to isotopic change demands that these tests be used in conjunction with other indicators, including $\delta^{13}C_{org}$ and evaluation of stratigraphic and isotopic patterns across facies and throughout regions. The Avzyan Formation of the Southern Urals has experienced significant post-depositional alteration, as evidenced by isotopic and trace element profiles; however, $\delta^{13}C$ values are preserved in multiple sections in different facies and are consistent with $\delta^{13}C_{org}$ values recovered from intercalated shales of the Kataskin Member. These lines of evidence indicate that $\delta^{13}C$ values of the Avzyan Formation preserve a seawater signal of carbon isotopic change through time.

Carbon isotope data from the Avzyan Formation show a pattern of moderately positive average $\delta^{13}C$ values that become increasingly positive upsection. This pattern is strikingly similar to that of the 1300–1270 Ma Dismal Lakes Group, and supports the hypothesis that both patterns record a global carbon isotopic signal. Although it is presently impossible to establish that the Avzyan Formation and the Dismal Lakes Group are coeval, their ages are likely to be broadly similar. Both units exhibit a style of variation that suggests that the transition between predominantly 0‰ values at 1300 Ma and +3.5‰ at 1250 Ma occurred as a series of pulses, rather than as a monotonic increase. Furthermore, Avzyan carbonates preserve a few highly positive (>+4‰) $\delta^{13}C$ values, suggestive of the post-1250 Ma steady state characterized by higher average $\delta^{13}C$ and greater isotopic variability, linked to global changes in carbon cycling and inorganic carbon reservoir size (Bartley and Kah, 2004).

Acknowledgements

The geologists of the Ufimian Geologic Institute made us welcome in the Urals and enthusiastically shared their numerous years of experience in this field area. Without them, the fieldwork could not have been a success. We thank Viktor N. Puchkov, Nina D.

Sergeeva, Peter N. Mikhailov, and Vachyslav I. Kozlov. Our interpreter, Larissa, provided an invaluable service to a group of people who lack fluency in the languages of their colleagues.

A.J. Kaufman and R. Walker from University of Maryland provided laboratory space and mass spectrometer time and assisted in $^{87}Sr/^{86}Sr$ analyses. M. Emmons (Mountain Mass Spectrometry) and D. Winter (University of California Davis) provided a number of stable isotopic analyses. We are also grateful to C Mora and Z.-H. Li for generously allowing us access to the stable isotope ratio mass spectrometer at University of Tennessee for the remaining stable isotopic analyses. We thank T. Lyons and J. Karhu for thoughtful reviews of this manuscript.

This project was funded by NASA Exobiology grant #NAG5-10666, National Geographic Society grant #6796-00, and a Faculty Research Grant from the University of West Georgia.

References

Anbar, A.D., Knoll, A.H., 2002. Proterozoic ocean chemistry and evolution: a bioinorganic bridge? Science 297, 1137–1142.

Banner, J.L., Hanson, G.N., 1990. Calculation of simultaneous isotopic and trace element variations during water–rock interaction with applications to carbonate diagenesis. Geochim. Cosmochim. Acta 54, 3123–3137.

Banner, J.L., Kaufman, J., 1994. The isotopic record of ocean chemistry and diagenesis preserved in non-luminescent brachiopods from Mississippian carbonate rocks, Illinois and Missouri. GSA Bull. 106, 1074–1082.

Bartley, J.K., Kah, L.C., 2004. Marine carbon reservoir, C_{org}–C_{carb} coupling, and the evolution of the Proterozoic carbon cycle. Geology 32, 129–132.

Bartley, J.K., Pope, M., Knoll, A.H., Petrov, P.Y., Semikhatov, M.A., Sergeev, V.N., 1998. A Precambrian–Cambrian boundary succession from the western Siberian Platform: geochemistry, stratigraphy, and paleontology. Geol. Mag. 135, 473–494.

Bartley, J.K., Knoll, A.H., Grotzinger, J.P., Sergeev, V.N., 2000. Lithification and fabric genesis in precipitated stromatolites and associated peritidal carbonates, Mesoproterozoic Billyakh Group, Siberia. In: Grotzinger, J.P., James, N.P. (Eds.), Carbonate Sedimentation and Diagenesis in the Evolving Precambrian World. SEPM Special Publication, vol. 67. SEPM (Society for Sedimentary Geology), Tulsa, pp. 59–73.

Bartley, J.K., Semikhatov, M.A., Kaufman, A.J., Knoll, A.H., Pope, M.C., Jacobsen, S.B., 2001. Global events across the Mesoproterozoic–Neoproterozoic boundary: C and Sr isotopic evidence from Siberia. Precambrian Res. 111, 165–202.

Brasier, M.D., Lindsay, J.F., 1998. A billion years of environmental stability and the emergence of eukaryotes: new data from northern Australia. Geology 26, 555–558.

Brasier, M.D., Shields, G., Kuleshov, V.N., Zhegallo, L.A., 1996. Integrated chemo-and biostratigraphic calibration of early animal evolution: Neoproterozoic–early Cambrian of southwest Mongolia. Geol. Mag. 133, 445–485.

Brown, D., Alvarez-Marron, J., Perez-Estaun, A., Gorozhanina, Y., Baryshev, V., Puchkov, V., 1997. Geometric and kinematic evolution of the foreland thrust and fold belt in the southern Urals. Tectonics 16, 551–562.

Buick, R., Des Marais, D.J., Knoll, A.H., 1995. Stable isotopic compositions of carbonates from the Mesoproterozoic Bangemall Group, northwestern Australia. Chem. Geol. 123, 153–171.

Butterfield, N.J., 2000. *Bangiomorpha pubescens* n. gen., n. sp.: implications for the evolution of sex, multicellularity, and the Mesoproterozoic/Neoproterozoic radiation of eukaryotes. Paleobiology 26, 386–404.

Butterfield, N.J., Knoll, A.H., Swett, K., 1990. A bangiophyte red alga from the Proterozoic of Arctic Canada. Science 250, 104–107.

Canfield, D.E., 1998. A new model for Proterozoic ocean chemistry. Nature 396, 450–453.

Canfield, D.E., Teske, A., 1996. Late Proterozoic rise in atmospheric oxygen concentration inferred from phylogenetic and sulphur-isotopic sudies. Nature 382, 127–132.

Craig, H., 1957. Isotopic standards for carbon and oxygen and correction factors for mass-spectrometric analysis of carbon dioxide. Geochim. Cosmochim. Acta 12, 133–149.

Dalziel, I.W.D., 1991. Pacific margins of Laurentia and East Antarctica–Australia as a conjugate rift pair: evidence and implications for an Eocambrian supercontinent. Geology 19, 598–601.

Derry, L.A., Kaufman, A.J., Jacobsen, S.B., 1992. Sedimentary cycling and environmental change in the Late Proterozoic: evidence from stable and radiogenic isotopes. Geochim. Cosmochim. Acta 56, 1317–1329.

Derry, L.A., Brasier, M.D., Corfield, R.M., Rozanov, A.Y., Zhuravlev, A.Y., 1994. Sr and C isotopes in Lower Cambrian carbonates from the Siberian craton: a paleoenvironmental record during the 'Cambrian explosion'. Earth Planet. Sci. Lett. 128, 671–681.

Des Marais, D.J., Strauss, H., Summons, R.E., Hayes, J.M., 1992. Carbon isotope evidence for the stepwise oxidation of the Proterozoic environment. Nature 359, 605–609.

Dromgoole, E.L., Walter, L.M., 1990. Iron and manganese incorporation into calcite: effects of growth kinetics, temperature, and solution chemistry. Chem. Geol. 81, 311–336.

Ellmies, R., Krupenin, M.T., Bogatov, V.I., Chplygina, N.V., 2000. Early–Middle Riphean age of the main diabase dike generation in Lower Riphean rocks of the Bakal Regions (Southern Urals). Ural. Br. Russ. Acad. Sci. 4, 228–230 (in Russian).

Fairchild, I.J., Marshall, J.D., Bertrand-Sarfati, J., 1990. Stratigraphic shifts in carbon isotopes from Proterozoic stromatolitic carbonates (Mauritania): influences of primary mineralogy and diagenesis. Am. J. Sci. 290-A, 46–79.

Frank, T.D., Lyons, T.W., 2000. The integrity of $\delta^{18}O$ records in Precambrian carbonates: a Mesoproterozoic case study. In: Grotzinger, J.P., James, N.P. (Eds.), Carbonate Sedimentation and Diagenesis in the Evolving Precambrian World. SEPM Special Publication, vol. 67. SEPM, Tulsa, pp. 315–326.

Frank, T.D., Lyons, T.W., Lohmann, K.C., 1997. Isotopic evidence for the paleoenvironmental evolution of the Mesoproterozoic Helena Formation, Belt Supergroup, Montana, USA. Geochim. Cosmochim. Acta 61, 5023–5041.

Frank, T.D., Kah, L.C., Lyons, T.W., 2003. Changes in organic matter production and accumulation as a mechanism for isotopic evolution in the Mesoproterozoic ocean. Geol. Mag. 140, 397–420.

Furniss, G., Rittel, J.F., Winston, D., 1998. Gas bubble and expansion crack origin of "molar-tooth" calcite structures in the middle Proterozoic Belt Supergroup, western Montana. J. Sediment. Res. 68, 104–114.

Giese, U., Glasmacher, U., Kozlov, V.I., Matenaar, I., Puchkov, V.N., Stroink, L., Ladage, S., Walter, R., 1999. Structural framework of the Bashkirian anticlinorium, SW Urals. Geol. Rundsc. 87, 526–544.

Glasmacher, U.A., Bauer, W., Giese, U., Reynolds, P., Kober, B., Puchkov, V., Stroink, L., Alekseyev, A., Willner, A.P., 2001. The metamorphic complex of Beloretzk, SW Urals, Russia— a terrane with polyphase Meso- to Neoproterozoic thermo-dynamic evolution. Precambrian Res. 110, 185–213.

Gorokhov, I.M., Melnikov, N.N., Turchenko, T.L., 1995a. Two illite generations in the Upper Riphean shale: the Rb–Sr isotope evidence. Terra Nova 7, 330–331.

Gorokhov, I.M., Semikhatov, M.A., Baskakov, A.V., Kutyavin, E.P., Mel'nikov, N.N., Sochava, A.V., Turchenko, T.L., 1995b. Sr isotopic composition in Riphean, Vendian, and Lower Cambrian carbonates from Siberia. Stratigr. Geol. Correl. 3, 1–28.

Gorozhanin, V.M., 1995. Rb–Sr method in resolving problems of the South Urals geology. Ural. Br. Russ. Acad. Sci. 1, 1–25.

Grotzinger, J.P., 1989. Facies and evolution of Precambrian carbonate depositional systems: emergence of the modern platform archetype. In: Crevello, P.D., Wilson, J.L., Sarg, J.F., Read, J.F. (Eds.), Controls on Carbonate Platform and Basin Development. SEPM Special Publication, vol. 44. Allen Press, Lawrence, pp. 79–106.

Halverson, 2006. Neoproterozoic Reference Curve paper.

Hoffman, P.F., 1989. Speculations on Laurentia's first gigayear (2.0 to 1.0 Ga). Geology 17, 135–138.

Hoffman, P.F., 1991. Did the breakout of Laurentia turn Gondwanaland inside–out? Science 252, 1409–1412.

Ivanov, S.N., Krasnobaev, A.A., Rusin, A.I., 1986. Geodynamic regimes in the Precambrian of the Urals. Precambrian Res. 33, 189–208.

James, N.P., Narbonne, G., Sherman, A., 1998. Molar-tooth carbonates: shallow subtidal facies of the mid-to late Proterozoic. J. Sediment. Res. 68, 716–722.

Kah, L.C., 2000. Depositional $\delta^{18}O$ signatures in Proterozoic dolostones: constraints on seawater chemistry and early diagenesis. In: Grotzinger, J.P., James, N.P. (Eds.), Carbonate Sedimentation and Diagenesis in the Evolving Precambrian World. SEPM Special Publication, vol. 67. SEPM, Tulsa, pp. 345–360.

Kah, L.C., Bartley, J.K., 1997. Establising a carbon isotopic reference curve for the Mesoproterozoic: biogeochemical links to the tectonic assembly of Rodinia. Geol. Soc. Am. Abstr. Programs 29, A-115.

Kah, L.C., Bartley, J.K., 2004. Growth dynamics of stromatolite reefs in the Proterozoic Atar Group, Mauritania. Geol. Soc. Am. Abstr. Programs 36, 111.

Kah, L.C., Knoll, A.H., 1996. Microbenthic distribution of Proterozoic tidal flats: environmental and taphonomic considerations. Geology 24, 79–82.

Kah, L.C., Bartley, J.K., Frank, T.D., Lyons, T.W., 1999a. Reef facies and possible chemosynthetic communities of the Sulky formation, ~1.3 Ga Dismal Lakes Group, NWT, Canada. Geological Association of Canada/Mineralogical Association of Canada, Annual Joint Meeting. Abstracts, vol. 24, p. 60.

Kah, L.C., Sherman, A.B., Narbonne, G.M., Kaufman, A.J., Knoll, A.H., James, N.P., 1999b. Isotope stratigraphy of the Mesoproterozoic Bylot Supergroup, Northern Baffin Island: implications for regional lithostratigraphic correlations. Can. J. Earth Sci. 36, 313–332.

Kah, L.C., Lyons, T.W., Chesley, J.T., 2001. Geochemistry of a 1.2 Ga carbonate–evaporite marine succession, northern Baffin and Bylot Islands: implications for Mesoproterozoic marine evolution. Precambrian Res. 111, 203–234.

Kah et al., 2004. NATURE PAPER.

Karlstrom, K.E., Åhall, K.-I., Harlan, S.S., Williams, M.L., McLelland, J., Geissman, J.W., 2001. Long-lived (1.8–1.0 Ga) convergent orogen in southern Laurentia, its extensions to Australia and Baltica, and implications for refining Rodinia. Precambrian Res. 111, 5–30.

Kaufman, A.J., Knoll, A.H., 1995. Neoproterozoic variations in the C-isotopic composition of seawater: stratigraphic and biogeochemical implications. Precambrian Res. 73, 27–49.

Kaufman, A.J., Hayes, J.M., Knoll, A.H., Germs, G.J.B., 1991. Isotopic compositions of carbonates and organic carbon from upper Proterozoic successions in Namibia: stratigraphic variation and the effects of diagenesis and metamorphism. Precambrian Res. 49, 301–327.

Kaufman, A.J., Jacobsen, S.B., Knoll, A.H., 1993. The Vendian record of Sr and C isotopic variations in seawater: implications for tectonics and paleoclimate. Earth Planet. Sci. Lett. 120, 409–430.

Kaufman, A.J., Knoll, A.H., Narbonne, G.M., 1997. Isotopes, ice ages, and terminal Proterozoic Earth history. Proc. Natl. Acad. Sci. U. S. A. 94, 6600–6605.

Keller, B.M., Chumakov, N.M., 1983. Stratotype of Riphean. Stratigraphy, Geochronology. Nauka, Moscow (in Russian).

Keller, B.M., Krasnobaev, A.A., 1983. Late Precambrian geochronology of the European part of the USSR. Geol. Mag. 120, 381–389.

Kerans, C., Donaldson, J.A., 1989. Deepwater conical stromatolite reef, Sulky Formation (Dismal Lakes Group), Middle Proterozoic, N.W.T. Can. Soc. Pet. Geol. Mem. 13, 81–88.

Knoll, A.H., 1992. The early evolution of eukaryotic organisms: a geological perspective. Science 256, 622–627.

Knoll, A.H., Kaufman, A.J., Semikhatov, M.A., 1995. The carbon isotopic composition of Proterozoic carbonates: Riphean successions from northwestern Siberia (Anabar Massif, Turukhansk uplift). Am. J. Sci. 295, 823–850.

Kozlov, V.I., Krasnobaev, A.A., Larionov, N.N., Maslov, A.V., Sergeeva, N.D., Ronkin, YuL., Bibikova, E.V., 1989. Lower Riphean of the Southern Urals. Nauka, Moscow (in Russian).

Kuznetsov, A.B., Ovchinnikova, G.V., Gorokhov, I.M., Kaurova, O. K., Krupenin, V.N., Maslov, A.V., 2003. Sr–isotope signature and Pb–Pb age of the Bakal Formation limestones in the lower Riphean type section, the Southern Urals. Dokl. Earth Sci. 391A (6), 819–822.

Land, L.S., 1980. The isotopic and trace element geochemistry of dolomite: the state of the art. In: Zenger, D.H., Dunham, J.B., Ethington, R.L. (Eds.), Concepts and Models of Dolomitization. SEPM, Tulsa, pp. 87–110.

LeCheminant, A.N., Heaman, L.M., 1989. Mackenzie igneous events, Canada: Middle Proterozoic hotspot magmatism associated with ocean opening. Earth Planet. Sci. Lett. 96, 38–48.

Lindsay, J.F., Brasier, M.D., 2000. A carbon isotope reference curve for ca. 1700–1575 Ma McArthur and Mount Isa basins, Northern Australia. Precambrian Res. 99, 271–308.

Maloof, A., 2005–6. Cambrian reference curve paper.

Maslov, A.V., 1989. Very shallow water depositional complexes in the Riphean of the southern Ural Mountains. Lithol. Miner. Resour. 24, 124–136.

Maslov, A.V., 1994. The Early Riphean Volga–Urals sedimentation basin. Lithol. Miner. Resour. 29, 486–502.

Maslov, A.V., 2002. Facies associations of Riphean sedimentary sequences. Lithol. Miner. Resour. 37, 462–473.

Maslov, A.V., Erdtmann, B.-D., Ivanov, S.N., Krupenin, M.T., 1997. The main tectonic events, depositional history, and the palaeogeography of the Southern Urals during the Riphean–Early Palaeozoic. Tectonophysics 276, 313–335.

Matenaar, I., Glasmacher, U.A., Pickel, W., Giese, U., Pazikhin, V.N., Kozlov, V.I., Puchkov, V.N., Stroink, L., Walter, R., 1999. Incipient metamorphism between Ufa and Beloretzk, western fold-and-thrust belt, southern Urals, Russia. Geol. Rundsch. 87, 545–560.

McKenzie, J.A., Hsü, K.J., Schneider, J.F., 1980. Movement of subsurface waters under the sabkha, AbuDhabi, UAE, and its relation to evaporative dolomite genesis. In: Zenger, D.H., Dunham, J.B., Ethington, R.L. (Eds.), Concepts and Models of Dolomitization. SEPM Special Publication, vol. 28. SEPM, Tulsa, pp. 11–30.

Montañez, I.P., Read, J.F., 1992. Eustatic control on early dolomitization of cyclic peritidal carbonates: evidence from the Early Ordovician Upper Knox Group, Appalachians. GSA Bull. 104, 872–886.

Montañez, I.P., Banner, J.L., Osleger, D.A., Borg, L.E., Bosserman, P.J., 1996. Integrated Sr isotope variations and sea-level history of Middle to Upper Cambrian platform carbonates; implications for the evolution of Cambrian seawater $^{87}Sr/^{86}Sr$. Geology 24, 917–920.

O'Connor, M.P., 1972. Classification and environmental interpretation of the cryptalgal organosedimentary "molar-tooth" structure from the Late Precambrian Belt-Purcell Supergroup. J. Geol. 80, 592–610.

Ovchinnikova, G.V., Vasil'eva, I.M., Semikhatov, M.A., Kuznetsov, A.B., Gorokhov, I.M., Gorokhovskii, B.M., Levskii, L.K., 1998. U–Pb systematics of Proterozoic carbonate rocks: the Inzer Formation of the Upper Riphean stratotype (Southern Urals). Stratigr. Geol. Correl. 6, 336–347.

Pollock et al., 2006. MT paper in JSR.

Rainbird, R.H., Stern, R.A., Khudoley, A.K., Kropachev, A.P., Heaman, L.M., Sukhorukov, V.I., 1998. U–Pb geochronology of Riphean sandstone and gabbro from southeast Siberia and its bearing on the Laurentia–Siberia connection. Earth Planet. Sci. Lett. 164, 409–420.

Rosenbaum, J., Sheppard, W.M.F., 1986. An isotopic study of siderites, dolomites, and ankerites at high temperatures. Geochim. Cosmochim. Acta 50, 1147–1150.

Roths, P.J., 1993. Geochemical and geochronological studies of the Grenville-age (1250–1000 Ma) Allamoore and Hazel formations, Hudspeth and Culberson Counties, West Texas. In: Soegaard, K., et al. (Ed.), Precambrian Geology of Franklin Mountains and Van Horn Area, Trans-Pecos, Texas, Geological Soceity of America Field Trip Guidebook. Geological Society of America, Boulder, pp. 11–35.

Saltzman, M.R., 2003. The Late Paleozoic ice age: oceanic gateway or pCO_2. Geology 31, 151–155.

Saltzman, M.R., Davidson, J.P., Holden, P., Runnegar, B., Lohmann, K.C., 1995. Sea-level-driven changes in ocean chemistry at an Upper Cambrian extinction horizon. Geology 23, 893–896.

Stiller, M., Rounick, J.S., Shasha, S., 1985. Extreme carbon-isotope enrichments in evaporating brines. Nature 316, 434–435.

Strauss, H., Des Marais, D.J., Hayes, J.M., Summons, R.E., 1992. Proterozoic organic carbon — its preservation and isotopic record. In: Schidlowski, M., Golubic, S., Kimberley, M.M., McKirdy, D.M., Trudinger, P.A. (Eds.), Early Organic Evolution: Implications for Mineral and Energy Resources. Springer-Verlag, Berlin, pp. 203–211.

Sumner, D.Y., Grotzinger, J.P., 1996a. Were kinetics of Archean calcium carbonate precipitation related to oxygen concentration? Geology 24, 119–122.

Sumner, D.Y., Grotzinger, J.P., 1996b. Herringbone calcite: petrography and environmental significance. J. Sediment. Res. 66, 419–429.

Willner, A.P., Ermaloaeva, T., Stroink, L., Glasmacher, U.A., Giese, U., Puchkov, V.N., Kozlov, V.I., Walter, R., 2001. Contrasting provenance signals in Riphean and Vendian sandstones in the SW Urals (Russia): constraints for a change from passive to active continental margin conditions in the Neoproterozoic. Precambrian Res. 110, 215–239.

Willner, A.P., Sindern, S., Metzger, R., Ermolaeva, T., Kramm, U., Puchkov, V., Kronz, A., 2003. Typology and single grain U/Pb ages of detrital zircons from Proterozoic sandstones in the SW Urals (Russia): early time marks at the eastern margin of Baltica. Precambrian Res. 124, 1–20.

Woods, K., Knoll, A.H., German, T., 1998. Xanthophyte algae from the Mesoproterozoic/Neoproterozoic transition: confirmation of evolutionary implications. Geol. Soc. Am. Abstr. Programs 30, A-232.

Xiao, X., Knoll, A.H., Kaufman, A.J., Yin, L., Yun, Z., 1997. Neoproterozoic fossils in Mesoproterozoic rocks? Chemostratigraphic resolution of a biostratigraphic conundrum from the North China Platform. Precambrian Res. 84, 197–220.